Models of the cytochromes b. Control of axial ligand orientation with a hindered porphyrin system

ARTICLE *in* JOURNAL OF THE AMERICAN CHEMICAL SOCIETY · JULY 1991

Impact Factor: 12.11 · DOI: 10.1021/ja00015a001

4 AUTHORS, INCLUDING:

Martin Safo
Virginia Commonwealth University
87 PUBLICATIONS **2,024** CITATIONS
SEE PROFILE

F(rances) Ann Walker
The University of Arizona
240 PUBLICATIONS **8,646** CITATIONS
SEE PROFILE

W. Robert Scheidt
University of Notre Dame
363 PUBLICATIONS **13,272** CITATIONS
SEE PROFILE

VOLUME 113, NUMBER 15
JULY 17, 1991

JOURNAL
OF THE
AMERICAN
CHEMICAL
SOCIETY

Models of the Cytochromes *b*. Control of Axial Ligand Orientation with a "Hindered" Porphyrin System

Martin K. Safo,[1] Govind P. Gupta,*[,2] F. Ann Walker,*[,3] and W. Robert Scheidt*[,1]

Contribution from the Department of Chemistry and Biochemistry, University of Notre Dame, Notre Dame, Indiana 46556, Department of Physics, The Pennsylvania State University, State College, Pennsylvania 16802, and Department of Chemistry, University of Arizona, Tucson, Arizona 85721. *Received October 19, 1990*

Abstract: The development of an iron porphyrinate/axial ligand system that leads to control of the relative and absolute axial ligand orientations is described. The system consists of the iron(III) complex of the hindered porphyrin *meso*-tetramesitylporphyrin and pyridine ligands. The preparation and characterization of the low-spin $[Fe(TMP)(4\text{-}NMe_2Py)_2]ClO_4$ (4-NMe_2Py = 4-(dimethylamino)pyridine) derivative is described. The crystal structure determination shows that the complex has the desired relative perpendicular orientation of the two axial pyridines. The two pyridine planes are close to eclipsing adjacent Fe–C_m vectors. The porphinato core is strongly S_4-ruffled; the Fe–N_p bonds show a commensurate shortening from the values expected for planar low-spin species. The EPR spectrum of the complex has a large g_{max} feature at 3.48 and no other discernible features. An analysis of the Mössbauer spectrum in a 6 T field allows estimation of a range of possible crystal field parameters (Δ/λ = 1.9–3.6, V/λ = 0.7–0.89). The complex displays the usual quadrupole doublet in zero field with an isomer shift of 0.20 and a quadrupole splitting of 1.74 mm/s. As discussed in the text, relatively low values of the quadrupole splitting constant appear characteristic of perpendicular orientations of the axial ligands in low-spin iron(III). Two "control" complexes have also been prepared and characterized. The crystal structure of the bis[4-(dimethylamino)pyridine] derivative of (octaethylporphinato)iron(III) shows that it has the normal parallel orientation of axial ligands and a normal low-spin rhombic EPR spectrum with g_z = 2.818, g_y = 2.275, and g_x = 1.630. Crystal field parameters for this complex have also been obtained from an analysis of the Mössbauer spectrum in a 6-T field. This complex also displays a quadrupole doublet in zero field with an isomer shift of 0.26 and quadrupole splitting of 2.14 mm/s. Bis(1-methylimidazole)(*meso*-tetramesitylporphinato)iron(III) has also been characterized; as expected, relative parallel orientations of axial ligands are found in the crystal structure as well as a planar porphyrin core. Mössbauer parameters are δ = 0.28 mm/s and ΔE_q = 2.28 mm/s. Crystal data: $[Fe(TMP)(4\text{-}NMe_2Py)_2]ClO_4 \cdot 2C_6H_5Cl$: a = 15.240 (3) Å, b = 25.800 (6) Å, c = 18.181 (4) Å, β = 97.72 (2)°, monoclinic, space group $P2_1/n$, V = 7083.7 Å^3, Z = 4, number of observed data = 6935, R_1 = 0.062, R_2 = 0.071. $[Fe(OEP)(4\text{-}NMe_2Py)_2]ClO_4 \cdot CH_2Cl_2$: a = 10.480 (6) Å, b = 10.692 (6) Å, c = 11.210 (4) Å, α = 84.04 (4)°, β = 85.88 (4)°, γ = 78.43 (6)°, triclinic, space group $P\bar{1}$, V = 1222.2 Å^3, Z = 1, number of observed data = 4105, R_1 = 0.067, R_2 = 0.086. $[Fe(TMP)(1\text{-}MeIm)_2]ClO_4$: a = 13.929 (2) Å, b = 14.430 (2) Å, c = 15.106 (3) Å, α = 94.02 (1)°, β = 106.97 (1)°, γ = 96.24 (1)°, triclinic, space group $P\bar{1}$, V = 2870.3 Å^3, Z = 2, number of observed data = 6276, R_1 = 0.046, R_2 = 0.054.

Introduction

There continues to be considerable interest in determining what factors affect the reduction potentials, electronic properties, and nuclear magnetic and electron paramagnetic resonance spectra, as well as other properties of heme proteins, and in developing an understanding of how these physical properties may relate to each other. Developing such relationships would be useful in achieving a complete understanding of the structural and electronic features of heme proteins. Previous studies have shown how substituents on the β-pyrrole positions in the *a*,*b*,*c*-type hemes[4]

(1) University of Notre Dame.
(2) The Pennsylvania State University. Present address: Department of Physics, Lucknow University, Lucknow, 226 007 India.
(3) University of Arizona.

(4) Falk, J. E. In *Porphyrins and Metalloporphyrins*; Elsevier: New York, 1964; p 70.

0002-7863/91/1513-5497$02.50/0

Table I. Summary of Crystal Data and Intensity Collection Parameters

complex	$[Fe(OEP)(4\text{-}NMe_2Py)_2]ClO_4 \cdot CH_2Cl_2$	$[Fe(TMP)(4\text{-}NMe_2Py)_2]ClO_4 \cdot 2C_6H_5Cl$	$[Fe(TMP)(1\text{-}MeIm)_2]ClO_4$
formula	$FeCl_3O_4N_8C_{51}H_{66}$	$FeCl_3O_4N_8C_{82}H_{82}$	$FeClO_4N_8C_{64}H_{64}$
fw	1017.35	1403.80	1120.57
space group	$P\bar{1}$	$P2_1/n$	$P\bar{1}$
T, K	118	118	293
a, Å	10.480 (6)	15.240 (3)	13.929 (2)
b, Å	10.692 (6)	25.800 (6)	14.430 (2)
c, Å	11.210 (4)	18.181 (4)	15.106 (3)
α, deg	84.04 (4)	90.00	94.02 (1)
β, deg	85.88 (4)	97.72 (2)	106.97 (1)
γ, deg	78.43 (6)	90.00	96.24 (1)
V, Å^3	1222.18	7083.73	2870.29
Z	1	4	2
no. obsd data	4105	6935	6276
D(obsd), g/cm^3	1.35[a]	1.31[a]	1.26[b]
D(calcd), g/cm^3	1.38[a]	1.32[a]	1.27[b]
R_1	0.067	0.062	0.046
R_2	0.086	0.071	0.054

[a] D(obsd) obtained at 294 K and D(calcd) obtained at 118 K. [b] D(obsd) obtained at 294 K and D(calcd) obtained at 293 K.

and in cytochrome b_5,[5] as well as the nature of the axial ligands bound to the heme in each particular protein,[6-10] affect the spectroscopic and redox properties of the hemoprotein. Even within a common set of heme substituents and axial ligands, the physical properties of heme proteins vary widely. An example of such variation is the group of cytochromes b and c that have histidines coordinated to both the fifth and sixth positions of the heme. Among the cytochromes b of this class are the well-characterized proteins cytochrome b_5 from liver[11-13] and erythrocytes[13-15] of higher animals, yeast flavocytochrome b_2,[16,17] and the b cytochrome of vertebrate sulfite oxidase,[18] all of whose heme centers have reduction potentials in the range 0 to +30 mV (vs SHE). These cytochromes also have well-characterized and very similar NMR spectra and EPR spectra characteristic of "class B" heme proteins, with $g_1 \simeq 2.9$, $g_2 \simeq 2.2$, and $g_3 \simeq 1.5$.[19-21] Also within this class of cytochromes b are a wide variety of membrane-bound proteins that are involved in the electron-transport chains of plants and animals, including those of mitochondrial complex III (sometimes called b_{566} and b_{562}), as well as chloroplast cytochromes b_6 and possibly b_{559}, all of which have been shown to have bis-histidine coordination to the heme.[22-25] However, these proteins have a wider range of reduction potentials than do the b_5 and b_2 group,[26-34] and they are all further characterized by a peculiar EPR signal having a large g_{max} feature[36] at $g \geq 3.3$ as the sole observable spectral feature.[28-35] We[37,38] and others[22,32,39,40] speculated that this signal could be due to the axial imidazole planes being maintained perpendicular to each other rather than nearly parallel as in cytochrome b_5.[11] In a combined study of the structures and EPR and Mössbauer spectra of several model heme complexes, we were able to show that the energy difference of the d orbital involved in the reduction of Fe(III) to Fe(II) could be of the order of λ, the spin–orbit coupling constant for low-spin Fe(III),[41] for complexes in which the axial imidazoles were in parallel vs perpendicular planes. With some assumptions in the conversion of orbital energy differences to expected differences in reduction potentials, we were able to estimate that parallel vs perpendicular ligand orientation could account for differences in reduction potentials of up to 50 mV,

(5) Lee, K.-B.; Jun, E.; LaMar, G. N.; Rezzano, I. N.; Pandey, R. K.; Smith, K. M.; Walker, F. A.; Buttlaire, D. H. *J. Am. Chem. Soc.* **1991**, *113*, 3576–83.
(6) Pierrot, M.; Hasar, R.; Frey, M.; Payan, F.; Astier, J.-P. *J. Mol. Biol.* **1982**, *257*, 14341–48.
(7) Higuchi, Y.; Bando, S.; Kusuniki, M.; Matsuura, Y.; Yasuoka, N.; Kakudo, M.; Yamanaka, T.; Yagi, T.; Inokuchi, H. *J. Biochem.* (Tokyo) **1981**, *89*, 1659–62.
(8) Mathews, F. S. *Prog. Biophys. Mol. Biol.* **1985**, *45*, 1–56.
(9) Weber, P. C.; Howard, A.; Xuong, N. H.; Salemme, F. R. *J. Mol. Biol.* **1981**, *153*, 399–424.
(10) Mathews, F. S.; Bethge, P.; Czerwinski, E. W. *J. Mol. Biol.* **1979**, *254*, 1699–706.
(11) Mathews, F. S.; Czerwinski, E. W.; Argos, P. In *The Porphyrins*; Dolphin, D., Ed.; Academic Press: New York, 1979; Vol. 7, pp 108–147.
(12) Weber, H.; Weiss, W.; Staudinger, H. *Hoppe-Seyler's Z. Physiol. Chem.* **1971**, *352*, 109–10.
(13) Walker, F. A.; Emrick, D.; Rivera, J. E.; Hanquet, B. J.; Buttlaire, D. H. *J. Am. Chem. Soc.* **1988**, *110*, 6234–40.
(14) Passon, P. G.; Reed, D. W.; Hultquist, D. E. *Biochim. Biophys. Acta* **1972**, *275*, 51–61.
(15) Iyanagi, T. *Biochemistry* **1977**, *16*, 2725–30.
(16) Keller, R.; Groudinsky, O.; Wüthrich, K. *Biochim. Biophys. Acta* **1973**, *328*, 233–38.
(17) Labeyrie, F.; Groudinsky, O.; Jacquot-Armand, Y.; Naslin, L. *Biochim. Biophys. Acta* **1966**, *128*, 492–503.
(18) Guiard, B.; Lederer, F. *J. Mol. Biol.* **1979**, *135*, 639–50.
(19) Watari, H.; Groudinsky, O.; Labeyrie, F. *Biochim. Biophys. Acta* **1967**, *131*, 589–92.
(20) Bois-Poltoratsky, R.; Ehrenberg, A. *Eur. J. Biochem.* **1967**, *2*, 361–65.
(21) Blumberg, W. E.; Peisach, J. In *Structure and Bonding of Macromolecules and Membranes*; Chance, B., Yonetani, T., Eds.; Academic: New York, 1971; p 215.
(22) Widger, W. R.; Cramer, W. A.; Herrmann, R. G.; Trebst, A. *Proc. Natl. Acad. Sci. U.S.A.* **1984**, *81*, 674–78.
(23) Babcock, G. T.; Widger, W. R.; Cramer, W. A.; Oertling, W. A.; Metz, J. G. *Biochemistry* **1985**, *24*, 3638–45.
(24) Knaff, D. B. *TIBS* **1989**, *14*, 159–160 and references therein.
(25) Scherer, S. *TIBS* **1990**, *15*, 458–462 and references therein.
(26) Erecinska, M.; Oshino, R.; Oshino, N.; Chance, B. *Arch. Biochem. Biophys.* **1973**, *157*, 431–45.
(27) Nelson, B. D.; Gellerfors, P. *Biochim. Biophys. Acta* **1974**, *357*, 358–64.
(28) Leigh, J. S.; Erecinska, M. *Biochim. Biophys. Acta* **1975**, *387*, 95–106.
(29) Von Jagow, G.; Schagger, H.; Engel, W. D.; Hachenberg, H.; Kolb, H. J. C. In *Energy Conservation in Biological Membranes*; Schafer, G., Klingenberg, M., Eds.; Springer: Berlin, 1978; pp 43–52.
(30) Salerno, J. C. *J. Biol. Chem.* **1984**, *259*, 2331–36.
(31) Tsai, A.-H.; Palmer, G. *Biochim. Biophys. Acta* **1983**, *722*, 349–63.
(32) Tsai, A.; Palmer, G. *Biochim. Biophys. Acta* **1982**, *681*, 484–95.
(33) Salerno, J. C. *FEBS Lett.* **1983**, *162*, 257–61.
(34) Malkin, R.; Vangard, T. *FEBS Lett.* **1980**, *111*, 228–31.
(35) Orme-Johnson, N. R.; Hansen, R. E.; Beinert, H. *J. Biol. Chem.* **1974**, *249*, 1928–39.
(36) This EPR spectral feature has also been termed HALS (highly anisotropic low-spin) and strong g_{max}. Both terminologies are somewhat misleading as greater anisotropy in the g tensor normally leads to a smaller calculated rhombicity V/Δ (complex is less rhombic, more tetragonal); moreover, the observed intensity of this spectral feature is very temperature dependent and in general the amplitude, in derivative mode, of the one observed feature is no greater than that of any one rhombic EPR signal at the same temperature.
(37) Scheidt, W. R.; Chipman, D. M. *J. Am. Chem. Soc.* **1986**, *108*, 163–67.
(38) Walker, F. A.; Reis, D.; Balke, V. L. *J. Am. Chem. Soc.* **1984**, *106*, 6888–98.
(39) Carter, K. R.; Tsai, A.; Palmer, G. *FEBS Lett.* **1981**, *132*, 243–46.
(40) Palmer, G. *Biochem. Soc. Trans.* **1985**, *13*, 548–60.
(41) Walker, F. A.; Huynh, B. H.; Scheidt, W. R.; Osvath, S. R. *J. Am. Chem. Soc.* **1986**, *108*, 5288–97.

with that of the perpendicular orientation being the more positive.[41] Recently, Huynh, Moura, Moura, and co-workers have found in a study of the bis-histidine-coordinated tetraheme bacterial cytochromes c_3 that axial ligand orientation can be correlated with reduction potential, with the potentials varying by 200 mV between the hemes having parallel- and perpendicular-oriented axial histidines.[42] They have explained this difference in reduction potential (larger than we had earlier predicted[41]) on the basis of a 4-fold multiplication of the energy differences of charge transfer as compared to d–d transition energies, as found by Thomson[43] in a study of the near-IR MCD spectra of a series of cytochromes. Thus, on the basis of very recent results,[42] it appears that axial ligand orientation may be an extremely important means of fine-tuning reduction potentials to specific values in particular cytochromes. In a continuing effort to determine what factors affect the choice of parallel vs perpendicular axial ligand plane alignment and to build models in which we can choose which form will exist, we have begun an extensive investigation of the axial ligand complexes of the so-called "hindered" metalloporphyrins having 2- and 6-phenyl substituents on all four phenyl rings.[44-54] These porphyrin ligands, which include tetrakis(2,6-dichlorophenyl)porphyrin (T2,6Cl_2PP) and tetramesitylporphyrin (TMP),[44] have been utilized in investigations of the oxo transfer chemistry of cytochrome P-450 model compounds[45-54] because they are able to prevent μ-oxo dimer formation[54] by providing a "pocket" to protect the metal oxene group. Nakamura and Groves[55] recently reported that one of these systems, when coordinated axially to two hindered imidazoles, [Fe(TMP)(2-MeHIm)$_2$]$^+$, showed apparent restricted rotation of the axial 2-methylimidazole ligands at low temperatures. We have found that these same porphyrin ligands provide interesting steric properties to the bis axially coordinated low-spin iron complexes that allow us to stabilize the perpendicular alignment—even in cases where we would not otherwise have expected to find it.

We have recently described the structure of the bis(1-vinylimidazole) complex of [*meso*-tetrakis(2,6-dichlorophenyl)porphinato]iron(III).[56] Although a desired ligand orientation was achieved in that work, in which half the molecules had their ligands in parallel planes and half in perpendicular planes, a detailed examination[56] suggests that it did not arise from true experimental control on our part. It is to be emphasized that an especially difficult aspect of controlling ligand orientation in model compounds is the concomitant need to ensure that a minimum of constraints, other than the desired ligand orientation, are incorporated into the experimental system. Thus, for example, the use of an elaborated porphyrin system with appended ligands would appear to be inappropriate; the two known solid-state structures[57,58] show unexpected stereochemical features that are plausibly interpreted as resulting from unintended constraints of the ligand appendage.

In this paper, we report that a slightly different experimental system can indeed be used to achieve a perpendicular relative orientation of the two axial ligands in iron(III) derivatives even when related, non-2,6-phenyl-substituted systems show a parallel relative orientation. The system consists of highly basic pyridine axial ligands and the "hindered" porphyrin ligand *meso*-tetramesitylporphyrin. The perpendicular orientation of the axial ligands results from the conjunction of steric effects of the pyridine ligands and the bulky ortho methyl phenyl substituents that must be fulfilled to achieve low-spin iron(III) complexes. The steric factors are specific for axial pyridine (six-membered ring) ligands as compared to nonhindered imidazoles (five-membered ring). We have previously shown that the bis complexes of basic pyridines such as 4-(dimethylamino)pyridine or 4-aminopyridine, like imidazoles, give "normal rhombic" EPR spectra.[38] On the basis of our earlier study of the structures and magnetic properties of imidazole complexes,[41] this suggests that in nonencumbered systems basic pyridines, like nonhindered imidazoles, favor parallel relative orientation of their axial ligand planes. In comparison, Strouse[59] has recently shown that the bisligand complex of iron(III) tetraphenylporphyrin with pyridine itself favors perpendicular relative orientation of the pyridine planes. Strouse found that for weak π donors such as pyridine itself, the spin–orbit splitting stabilizes the perpendicular geometry, whereas for strong π donors such as imidazoles the crystal field splitting (in units of λ) stabilizes the parallel geometry.[59] We report herein the structure and Mössbauer and EPR spectra of the complex [Fe(TMP)(4-NMe_2Py)$_2$]ClO_4,[44] an example in which a relative perpendicular orientation is stabilized but where parallel orientation would otherwise have been expected. We also report the same characterization of two control complexes, [Fe(OEP)(4-NMe_2Py)$_2$]ClO_4 and [Fe(TMP)(1-MeIm)$_2$]ClO_4, that confirms the basic mechanism for control of ligand orientation. One of our long-range goals in investigating these systems is to utilize them to investigate the effects of axial ligand plane orientation on reduction potentials of model compounds in homogeneous solution. The results of the present study will be of value to us in that endeavor.

Experimental Section

General Information. All solvents were distilled under argon prior to use. THF was distilled from sodium benzophenone ketyl. Dichloromethane, chlorobenzene, and hexane were distilled from CaH_2. 4-(Dimethylamino)pyridine and 1-methylimidazole were obtained from Ald-

(42) Ravi, N.; Moura, I.; Costa, C.; Teixeira, M.; LeGall, J.; Moura, J. G.; Huynh, B. H. *J. Am. Chem. Soc.*, submitted for publication.

(43) Gadsby, P. M. A.; Thomson, A. J. *J. Am. Chem. Soc.* **1990**, *112*, 5003–11. Makinen, M. W.; Curg, A. K. In *Iron Porphyrins, Part One*; Lever, A. B. P., Gray, H. B., Eds.; Addison-Wesley: Reading, MA, 1983; pp 141–230.

(44) Abbreviations used include 1-MeIm, 1-methylimidazole; 4-MeIm, 4-methylimidazolate; 4-MeHIm, 4-methylimidazole; 1-BzlIm, 1-benzylimidazole; 1,2-Me_2Im, 1,2-dimethylimidazole; 2-MeHIm, 2-methylimidazole; 5,6-Me_2BzHIm; 5,6-dimethylbenzimidazole; 1-VinIm, 1-vinylimidazole; 4-PhHIm, 4-phenylimidazole; HIm, imidazole; *c*-MU and *t*-MU, *cis*- and *trans*-methyl urocanate (methyl 4-imidazoleacrylate), respectively; 4-NMe_2Py, 4-(dimethylamino)pyridine; Py, pyridine; 4-MePy, 4-methylpyridine; 4-NH_2Py, 4-aminopyridine; 3,4-$(NH_2)_2$Py, 3,4-diaminopyridine; 3-Me,4-NMe_2Py, 3-methyl-4-(dimethylamino)pyridine; 3,4-Me_2Py, 3,4-dimethylpyridine; 3,5-Me_2,4-NMe_2Py, 3,5-dimethyl-4-(dimethylamino)pyridine; 2-quin, 2-quinoline; 3-Etpy, 3-ethylpyridine; 4-CNPy, 4-cyanopyridine; 3-ClPy, 3-chloropyridine; OEP, dianion of octaethylporphyrin; TPP, dianion of *meso*-tetraphenylporphyrin; TMP, dianion of *meso*-tetramesitylporphyrin; Proto IX, dianion of protoporphyrin IX; Proto IX DME, dianion of protoporphyrin IX dimethyl ester; T2,6-Cl_2PP, dianion of *meso*-tetrakis(2,6-dichlorophenyl)porphyrin; Tp-ClPP, *meso*-tetrakis(*p*-chlorophenyl)porphyrin; Tp-OCH_3PP, *meso*-tetra-*p*-methoxyporphyrin; TpivPP, *meso*-$\alpha,\alpha,\alpha,\alpha$-tetrakis(*o*-pivalamidophenyl)porphyrin (picket fence porphyrin); 18C6, 1,4,7,10,13,16-hexaoxacyclooctadecane (18-crown-6); 222, 4,7,13,16,21,24-hexaoxa-1,10-diazabicyclo[8.8.8]hexacosane (Kriptofix 222); N_p, porphinato nitrogen; N_{ax}, axial ligand nitrogen atom.

(45) Traylor, P. S.; Dolphin, D.; Traylor, T. G. *J. Chem. Soc., Chem. Commun.* **1984**, 279–80. Traylor, T. G.; Tsuchiya, S. *Inorg. Chem.* **1987**, *26*, 1338–39. Traylor, T. G.; Tsuchiya, S. *Inorg. Chem.* **1988**, *27*, 4520. Traylor, T. G.; Xu, F. *J. Am. Chem. Soc.* **1988**, *110*, 1953–58. Traylor, T. G.; Nakano, T.; Miksztal, A. R.; Dunlap, B. E. *Ibid.* **1986**, *108*, 7861–62.

(46) Artaud, I.; Devocelle, L.; Battioni, J. P.; Girault, J.-P.; Mansuy, D. *J. Am. Chem. Soc.* **1987**, *109*, 3782–83.

(47) Traylor, T. G.; Miksztal, A. R. *J. Am. Chem. Soc.* **1987**, *109*, 2770–74.

(48) Groves, J. T.; Stern, M. K. *J. Am. Chem. Soc.* **1988**, *110*, 8628–36.

(49) Rodgers, K. R.; Goff, H. M. *J. Am. Chem. Soc.* **1988**, *110*, 7049–60.

(50) Sugimoto, H.; Tung, H.-C.; Sawyer, D. T. *J. Am. Chem. Soc.* **1988**, *110*, 2465–70.

(51) Gold, A.; Jayaraj, K.; Doppelt, P.; Weiss, R.; Chottard, G.; Bill, E.; Ding, X.; Trautwein, A. X. *J. Am. Chem. Soc.* **1988**, *110*, 5756–61.

(52) Garrison, J. M.; Bruice, T. C. *J. Am. Chem. Soc.* **1989**, *111*, 191–8. Balasubramanian, P. N.; Lindsey Smith, J. R.; Davies, M. J.; Kaaret, T. W.; Bruice, T. C. *Ibid.* **1989**, *111*, 1477–83. Balasubramanian, P. N.; Lee, R. W.; Bruice, T. C. *Ibid.* **1989**, *111*, 8714–21. Pancucci, R.; Bruice, T. C. *Ibid.* **1990**, *112*, 6063–71. Murata, K.; Pancucci, R.; Gopinath, E.; Bruice, T. C. *Ibid.* **1990**, *112*, 6072–83.

(53) Collman, J. P.; Hampton, P. D.; Brauman, J. I. *J. Am. Chem. Soc.* **1990**, *112*, 2977–86, 2986–98.

(54) Cheng, R.-T.; Latos-Grazynski; Balch, A. L. *Inorg. Chem.* **1982**, *21*, 2412–18.

(55) Nakamura, M.; Groves, J. T. *Tetrahedron* **1988**, *44*, 3225–30.

(56) Hatano, K.; Safo, M. K.; Walker, F. A.; Scheidt, W. R. *Inorg. Chem.* **1991**, *30*, 1643–50.

(57) Mashiko, T.; Marchon, J.-C.; Musser, D. T.; Reed, C. A.; Kastner, M. E.; Scheidt, W. R. *J. Am. Chem. Soc.* **1979**, *101*, 3653–55.

(58) Bobrik, M. A.; Walker, F. A. *Inorg. Chem.* **1980**, *19*, 3383–90.

(59) Inniss, D.; Soltis, S. M.; Strouse, C. E. *J. Am. Chem. Soc.* **1988**, *110*, 5644–50.

rich and used without further purification. *meso*-Tetramesitylporphyrin was prepared by the method of Lindsey et al.[60] with slight modifications. A 2-L portion of $CHCl_3$ was measured into a 5-L three-necked round-bottom flask, equipped with a condenser and argon inlet and outlet ports. Mesitaldehyde (2.95 mL, 20 mmol) and freshly distilled pyrrole (1.39 mL, 20 mmol) were added. The solution was purged with argon for about 30 min. BF_3–etherate (2.64 mL, 6.6 mmol) (used as obtained, Aldrich) was added via syringe. After 1 h, *p*-chloranil (3.69 g, 15 mmol) was added and the reaction mixture was gently refluxed (45–50 °C) for 90 min. The reaction mixture was then cooled to room temperature. Triethylamine (920 μL, 6.6 mmol) was then added, and the solution was taken to dryness. Methanol (about 300 mL) was then added to the solid material, and the solution left for not less than 30 h. The purple crystals were collected by filtration and washed with methanol until the filtrate was colorless. The filtrate was left to stand for another 24 h for a second crop of crystals. The yield of the tetramesitylporphyrin varied between 20 and 32%. $[Fe(OEP)OClO_3]$ and $[Fe(TMP)OClO_3]$ were prepared by the method of Ogoshi et al.[61] THF was used instead of benzene as the solvent. $[Fe(OEP)OClO_3]$ was also prepared by the method of Dolphin et al.[62] Mössbauer spectroscopy samples were prepared from crushed single crystals as wax suspensions (mp 78 °C). Mössbauer measurements were made at 4.2 and/or 77 K, and in some cases with applied magnetic field as described previously.[63] EPR spectra were obtained on a Varian E-12 EPR spectrometer at San Francisco State University at 77 K, utilizing a Varian flowing nitrogen temperature controller, or down to 5 K, utilizing an Air Products Helitran liquid helium temperature controller. UV–vis spectra were recorded on a Perkin-Elmer Lambda 4C spectrometer and IR spectra on a Perkin-Elmer 883 spectrometer as KBr pellets.

Synthesis of $[Fe(OEP)(4\text{-}NMe_2Py)_2]ClO_4$. $[Fe(OEP)(4\text{-}NMe_2Py)_2]ClO_4$ was prepared by dissolving 40 mg (0.058 mmol) of $[Fe(OEP)OClO_3]$ and 42 mg (0.344 mmol) of $4\text{-}NMe_2Py$ in 15 mL of CH_2Cl_2. The reaction mixture was warmed for about 2 min with stirring. The solution was filtered and then divided into two portions. A mixture of hexane and CH_2Cl_2 (2:1 or 1:1) was allowed to diffuse into the solution. X-ray-quality crystals were obtained in 2 days.

Synthesis of $[Fe(TMP)(4\text{-}NMe_2Py)_2]ClO_4$. This was prepared with $[Fe(TMP)OClO_3]$ (50 mg, 0.053 mmol) and $4\text{-}NMe_2Py$ (100 mg, 0.819 mmol) dissolved in about 25 mL of chlorobenzene. The solution was warmed for about 2 min with stirring. The solution was filtered and layered with hexane. X-ray-quality crystals formed after 5 days.

Synthesis of $[Fe(TMP)(1\text{-}MeIm)_2]ClO_4$. $[Fe(TMP)OClO_3]$ (50 mg, 0.053 mmol) and 1-MeIm (100 mg, 1.22 mmol) were dissolved in about 25 mL of chlorobenzene. Reaction and crystallization procedures were as above. X-ray-quality crystals formed after 8 days.

Structure Determinations. All three crystalline complexes, $[Fe(OEP)(4\text{-}NMe_2Py)_2]ClO_4$, $[Fe(TMP)(4\text{-}NMe_2Py)_2]ClO_4$, and $[Fe(TMP)(1\text{-}MeIm)_2]ClO_4$, were examined on an Enraf-Nonius CAD4 diffractometer. All measurements utilized graphite-monochromated Mo Kα radiation (λ = 0.71073 Å). Final cell constants and complete details of the intensity collection and least-squares refinement parameters for the complexes are summarized in Tables I and SI (supplementary material). Four standard reflections were measured during each data collection; no significant fluctuations in intensities were noted. Intensity data were reduced with use of the profile fitting algorithm of R. H. Blessing.[64] All data with $F_o > 3.0\sigma(F_o)$ were retained as observed and used in all subsequent least-squares refinement.

The centrosymmetric space group $P\bar{1}$ was assumed for $[Fe(TMP)(1\text{-}MeIm)_2]ClO_4$ and $[Fe(OEP)(4\text{-}NMe_2Py)_2]ClO_4$; this choice was consistent with all subsequent developments of structure solution and refinement. The space group $P2_1/n$ for $[Fe(TMP)(4\text{-}NMe_2Py)_2]ClO_4$ is uniquely defined by the systematic absences. All three structures were determined with the direct methods program MULTAN.[65] For each, more than 80% of the atoms were found in the *E* map. The MULTAN output for $[Fe(TMP)(1\text{-}MeIm)_2]ClO_4$ suggested two independent special iron positions at 0, 0, 0 and $^1/_2$, $^1/_2$, $^1/_2$. There are thus two independent half-molecules, each with inversion symmetry, in the asymmetric unit of structure. With one molecule per unit cell, the $[Fe(OEP)(4\text{-}NMe_2Py)_2]ClO_4$ molecule also has a required center of symmetry. However, there is a full independent molecule in the asymmetric unit of $[Fe(TMP)(4\text{-}NMe_2Py)_2]ClO_4$. Subsequent difference Fourier syntheses for the three structures led to the location of the remaining atoms including the perchlorate anions and solvent molecules. Structure analyses were straightforward except for disorder of the perchlorate anion and CH_2Cl_2 solvent in $[Fe(OEP)(4\text{-}NMe_2Py)_2]ClO_4$ and a chlorobenzene solvent in $[Fe(TMP)(4\text{-}NMe_2Py)_2]ClO_4$. The methylene chloride and perchlorate in $[Fe(OEP)(4\text{-}NMe_2Py)_2]ClO_4$ alternatively both occupied the same site with the carbon atom of the methylene chloride and the chlorine of the perchlorate having approximately the same coordinates. These two statistically overlapped atoms were refined by using an average scattering factor $f_{Cl,C} = [f_{Cl} + f_C]/2$. In $[Fe(TMP)(4\text{-}NMe_2Py)_2]ClO_4$, one of the two chlorobenzene solvent molecules was disordered in two positions. One position was included in the full-matrix least-squares refinement with atomic occupancies of 0.8. The other position was refined by rigid-group methods; a six-membered ring with C–C distances of 1.380 Å and C–Cl distance of 1.72 Å with occupancies of 0.2 was used.

At the end of isotropic refinement, difference Fourier syntheses suggested possible locations of the hydrogen atoms in all complexes with the exception of those of the disordered solvent molecules. It should be emphasized that the rotational orientations of all methyl groups could be established. The hydrogen atom positions were idealized and included in subsequent cycles of least-squares refinement as fixed contributors (C–H = 0.95 Å and $B(H) = 1.3B(C)$), with additional reidealization as required. All three structures were refined to convergence with anisotropic temperature factors for all heavy atoms except the carbons of the disordered chlorobenzene solvent molecule in $[Fe(TMP)(4\text{-}NMe_2Py)_2]ClO_4$. Final atomic coordinates are listed in Tables II–IV. Included as supplementary material are the final anisotropic temperature factors and hydrogen atom positions for the complexes and the fixed atom positions

Table II. Fractional Coordinates of $[Fe(OEP)(4\text{-}NMe_2Py)_2]ClO_4\cdot CH_2Cl_2$[a]

atom	x	y	z
Fe	0.0000	0.0000	0.0000
N(1)	−0.0553 (3)	0.1905 (3)	−0.0323 (3)
N(2)	−0.1807 (3)	−0.0092 (3)	0.0656 (3)
N(3)	−0.0524 (3)	−0.0222 (3)	−0.1629 (3)
N(4)	−0.1610 (4)	−0.0668 (4)	−0.5071 (3)
C(a1)	0.0206 (4)	0.2729 (3)	−0.0871 (3)
C(a2)	−0.1769 (4)	0.2648 (3)	−0.0127 (3)
C(a3)	−0.2869 (4)	0.0910 (4)	0.0746 (3)
C(a4)	−0.2270 (4)	−0.1177 (4)	0.1067 (3)
C(b1)	−0.0562 (4)	0.4011 (4)	−0.1058 (3)
C(b2)	−0.1778 (4)	0.3956 (4)	−0.0582 (3)
C(b3)	−0.4025 (4)	0.0427 (4)	0.1217 (3)
C(b4)	−0.3655 (4)	−0.0864 (4)	0.1393 (3)
C(m1)	0.1533 (4)	0.2397 (4)	−0.1182 (3)
C(m2)	−0.2841 (4)	0.2184 (4)	0.0404 (3)
C(11)	−0.0092 (4)	0.5128 (4)	−0.1755 (4)
C(21)	−0.2963 (4)	0.5011 (4)	−0.0580 (4)
C(31)	−0.5360 (4)	0.1234 (4)	0.1441 (4)
C(41)	−0.4486 (4)	−0.1839 (4)	0.1840 (4)
C(12)	−0.0220 (5)	0.5097 (5)	−0.3106 (4)
C(22)	−0.3883 (4)	0.4950 (4)	−0.1572 (5)
C(32)	−0.5572 (4)	0.1674 (4)	0.2711 (4)
C(42)	−0.4465 (4)	−0.2197 (5)	0.3183 (4)
C(1)	−0.1572 (4)	0.0539 (4)	−0.2135 (3)
C(2)	−0.1961 (4)	0.0424 (4)	−0.3260 (4)
C(3)	−0.1267 (4)	−0.0541 (4)	−0.3957 (3)
C(4)	−0.0176 (4)	−0.1342 (4)	−0.3424 (3)
C(5)	0.0142 (4)	−0.1143 (4)	−0.2303 (4)
C(6)	−0.0984 (5)	−0.1760 (5)	−0.5712 (4)
C(7)	−0.2726 (4)	0.0187 (5)	−0.5604 (4)
Cl(C)	0.32093 (26)	−0.42656 (23)	−0.43008 (24)
Cl(1)	0.29279 (25)	−0.3901 (3)	−0.28457 (23)
Cl(2)	0.24991 (29)	−0.3626 (3)	−0.53985 (25)
O(1)	0.2187 (11)	−0.3275 (9)	−0.4807 (13)
O(2)	0.2875 (14)	−0.4690 (16)	−0.3088 (11)
O(3)	0.3301 (9)	−0.5334 (8)	−0.5023 (9)
O(4)	0.4352 (10)	−0.3838 (9)	−0.4359 (8)

[a] The estimated standard deviations of the least significant digits are given in parentheses.

(60) Wagner, R. W.; Lawrence, D. S.; Lindsey, J. S. *Tet. Lett.* **1987**, *28*, 3069–70. Lindsey, J. S.; Wagner, R. W. *J. Org. Chem.* **1988**, *54*, 828–36.
(61) Ogoshi, H.; Watanabe, E.; Yoshida, Z. *Chem. Lett.* **1973**, 989–92.
(62) Dolphin, D. H.; Sams, J. R.; Tsin, T. B. *Inorg. Chem.* **1977**, *16*, 711–13.
(63) Scheidt, W. R.; Osvath, S. R.; Lee, Y. J.; Reed, C. A.; Schaevitz, B.; Gupta, G. P. *Inorg. Chem.* **1989**, *28*, 1591–95.
(64) Blessing, R. H. *Cryst. Rev.* **1987**, *1*, 3–58.
(65) Programs used in this study included local modifications of Main, Hull, Lessinger, Germain, Declerq, and Woolfson's MULTAN, Jacobson's ALLS, Zalkin's FORDAP, Busing and Levy's ORFFE, and Johnson's ORTEP2. Atomic form factors were from: Cromer, D. T.; Mann, J. B. *Acta Crystallogr., Sect. A* **1968**, *A24*, 321–23. Real and imaginary corrections for anomalous dispersion in the form factor of the iron atom were from: Cromer, D. T.; Liberman, D. J. *J. Chem. Phys.* **1970**, *53*, 1891–98. Scattering factors for hydrogen were from: Stewart, R. F.; Davidson, E. R.; Simpson, W. T. *Ibid.* **1965**, *42*, 3175–87.

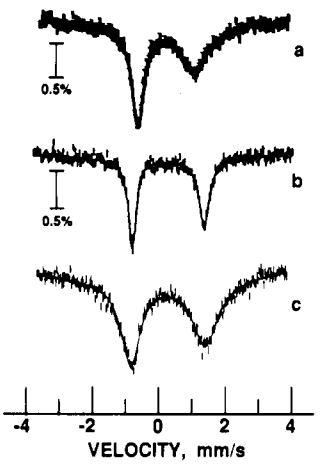

Figure 1. Mössbauer spectra of (a) $[Fe(TMP)(4\text{-}NMe_2Py)_2]ClO_4$, (b) $[Fe(OEP)(4\text{-}NMe_2Py)_2]ClO_4$, and (c) $[Fe(TMP)(1\text{-}MeIm)_2]ClO_4$ all recorded at 77 K in zero field. The solid line in each case is a two-Lorentzian fit of the data.

and group parameters for the chlorobenzene molecule of $[Fe(TMP)(4\text{-}NMe_2Py)_2]ClO_4$.

Results

The complexes have been characterized by IR, UV–vis, EPR, and Mössbauer spectroscopy and single-crystal X-ray structure determinations. The EPR spectrum of $[Fe(TMP)(4\text{-}NMe_2Py)_2]ClO_4$, recorded at 5 K, exhibits a large g_{max} signal at $g = 3.48$ with no other discernible features. The EPR spectrum of crystalline $[Fe(TMP)(1\text{-}MeIm)_2]ClO_4$ consists of several overlapping rhombic low-spin EPR signals that cannot be uniquely assigned. The overlapping spectra are presumably the result of differing absolute orientations of the axial imidazoles; two sets of rhombic signals would have been expected on the basis of the solid-state structure (vide infra). The EPR spectrum of $[Fe(OEP)(4\text{-}NMe_2Py)_2]ClO_4$, recorded at 24 K, shows a normal low-spin spectrum. The g values are summarized in Table V along with values for several other low-spin complexes for comparison.[38,41,59,66–69]

Figure 1a shows the Mössbauer spectrum of $[Fe(TMP)(4\text{-}NMe_2Py)_2]ClO_4$ at 77 K (zero field); parts b and c of Figure 1 show the corresponding 77 K spectra of the two control complexes of this study. At 4.2 K in zero applied field, the relaxation rate decreases so that the quadrupole doublet of $[Fe(TMP)(4\text{-}NMe_2Py)_2]ClO_4$ broadens. Application of a 6-T magnetic field resolves the hyperfine components of the Mössbauer spectrum at 4.2 K, as shown in Figure 2a. The isomer shift and quadrupole splitting obtained from the 77 K spectrum are given in Table VI. Included for comparison and subsequent discussion are the Mössbauer parameters of several other low-spin heme complexes that have been previously measured.[41,70–73] The asymmetry observed at 77 K is typical of species having intermediate relaxation effects.

The magnetic Mössbauer spectrum can be analyzed by using the theory developed by Griffith[74] and extended by Lang and co-workers[75,76] and Taylor.[77] In this theory, the electron configuration of low-spin Fe(III) is $(d_{xy})^2(d_{xz},d_{yz})^3$, which, even in equatorially symmetrical metalloporphyrins with perpendicularly bound planar axial ligands, exists as a rhombically distorted system, with tetragonal splitting parameter Δ and rhombic splitting parameter V. The two wave functions (for α and β spins) are thus linear combinations of the three states with coefficients a (for d_{yz}), b (for d_{xz}), and c (for d_{xy}); the e_g symmetry d orbitals are considered too high in energy to contribute to the wave functions. When the axis system of Taylor[77] is used, it can be shown that

$$g_x = 2[a^2 - (b + c)^2] \qquad g_y = 2[(a + c)^2 - b^2]$$
$$g_z = 2[(a + b)^2 - c^2] \tag{1}$$

The crystal field parameters V/λ and Δ/λ may be expressed as

$$V/\lambda = E_{yz} - E_{xz} = g_x/(g_z + g_y) + g_y/(g_z - g_x)$$

and

$$\Delta/\lambda = E_{yz} - E_{xy} - \tfrac{1}{2}V/\lambda = g_x/(g_z + g_y) + g_z/(g_y - g_x) - \tfrac{1}{2}V/\lambda \tag{2}$$

The equations for the hyperfine coupling constants originally derived by Lang and co-workers[75,76] may likewise be formulated from the wave functions and the axis system of Taylor[77] as

$$A_x = -P[-4bc - (1 + \kappa)(a^2 - b^2 - c^2) + \tfrac{3}{7}(a^2 - 3b^2 - 3c^2) + \tfrac{6}{7}a(b + c)]$$

$$A_y = P[-4ac - (1 + \kappa)(b^2 - a^2 - c^2) + \tfrac{3}{7}(b^2 - 3a^2 - 3c^2) + \tfrac{6}{7}b(a + c)]$$

$$A_z = P[-4ab - (1 + \kappa)(c^2 - a^2 - b^2) + \tfrac{3}{7}(c^2 - 3a^2 - 3b^2) + \tfrac{6}{7}c(a + b)] \tag{3}$$

where $P = -2g^*_N\mu_N\beta_e\langle r^{-3}\rangle_{3d}$ and κ is the Fermi contact constant.[79] $P = -4.2$ mm/s, $P/g^*_N\mu_N = -620$ kG, and $\kappa = 0.35$ for most heme proteins.[78]

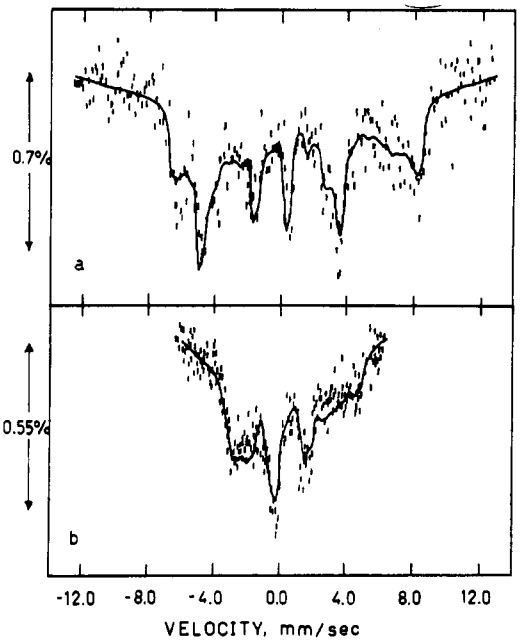

Figure 2. Mössbauer spectra of (a) $[Fe(TMP)(4\text{-}NMe_2Py)_2]ClO_4$ and (b) $[Fe(OEP)(4\text{-}NMe_2Py)_2]ClO_4$ recorded at 4.2 K in a 6-T applied magnetic field. The solid lines in each case represent the best fit to eq 4, obtained as described in the text.

(66) Scheidt, W. R.; Osvath, S. R.; Lee, Y. J. *J. Am. Chem. Soc.* **1987**, *109*, 1958–63.
(67) Higgins, T.; Safo, M. K.; Scheidt, W. R. *Inorg. Chim. Acta* **1991**, *178*, 261–67.
(68) Quinn, R.; Valentine, J. S.; Byrn, M. P.; Strouse, C. E. *J. Am. Chem. Soc.* **1987**, *109*, 3301–08.
(69) Quinn, R.; Strouse, C. E.; Valentine, J. S. *Inorg. Chem.* **1983**, *22*, 3934–40.
(70) Epstein, L. M.; Straub, D. K.; Maricondi, C. *Inorg. Chem.* **1967**, *6*, 1720–24.
(71) Bullard, L.; Panayappan, R. M.; Thorpe, A. N.; Hambright, P. *Bioinorg. Chem.* **1974**, *3*, 161–64.
(72) Medhi, O. K.; Silver, J. *J. Chem. Soc., Dalton Trans.* **1990**, 263–70.
(73) Straub, D. K.; Connor, W. M. *Ann. N.Y. Acad. Sci.* **1973**, *206*, 383–95.
(74) Griffith, J. S. *Proc. R. Soc. London, A* **1956**, *235*, 23–36.
(75) Oosterhuis, W. T.; Lang, G. *Phys. Rev.* **1969**, *178*, 439–56.
(76) Lang, G.; Marshall, W. *Proc. Phys. Soc.* **1966**, *87*, 3–34.
(77) Taylor, C. P. S. *Biochim. Biophys. Acta* **1977**, *491*, 137–148.
(78) Lang, G. *Q. Rev. Biophys.* **1970**, *3*, 1–60.
(79) Lang, G.; Dale, B. W. *Nucl. Instrum. Methods* **1974**, *116*, 567–71.

Table III. Fractional Coordinates of $[Fe(TMP)(4\text{-}NMe_2Py)_2]ClO_4 \cdot 2C_6H_6Cl$[a]

atom	x	y	z	atom	x	y	z
Fe	0.06016 (5)	0.162 354 (28)	0.243 36 (4)	C(33)	−0.2998 (3)	0.070 93 (20)	0.021 78 (27)
N(1)	0.07339 (25)	0.199 09 (15)	0.339 13 (20)	C(34)	−0.3178 (3)	0.018 56 (20)	0.016 07 (28)
N(2)	0.15034 (25)	0.206 77 (15)	0.209 75 (21)	C(35)	−0.2605 (3)	−0.015 33 (19)	0.058 83 (28)
N(3)	0.04786 (25)	0.125 21 (15)	0.148 12 (21)	C(36)	−0.1876 (3)	0.002 54 (19)	0.105 98 (26)
N(4)	−0.03175 (25)	0.117 62 (15)	0.276 74 (22)	C(37)	−0.2096 (3)	0.147 99 (19)	0.071 26 (27)
N(5)	−0.03322 (25)	0.212 74 (15)	0.203 94 (21)	C(38)	−0.3939 (4)	−0.000 64 (23)	−0.039 3 (3)
N(6)	0.15130 (25)	0.111 85 (15)	0.284 83 (21)	C(39)	−0.1246 (3)	−0.035 29 (20)	0.149 79 (28)
N(7)	−0.23612 (27)	0.314 22 (17)	0.116 71 (24)	C(41)	−0.0302 (3)	0.124 94 (19)	0.484 57 (27)
N(8)	0.32241 (28)	0.001 97 (18)	0.397 26 (25)	C(42)	0.0188 (3)	0.085 37 (20)	0.523 70 (27)
C(a1)	0.0438 (3)	0.182 12 (20)	0.403 40 (26)	C(43)	0.0070 (3)	0.075 63 (21)	0.597 31 (29)
C(a2)	0.1164 (3)	0.245 54 (19)	0.355 91 (27)	C(44)	−0.0525 (4)	0.103 80 (21)	0.633 03 (28)
C(a3)	0.1820 (3)	0.253 19 (19)	0.241 30 (26)	C(45)	−0.1044 (4)	0.140 17 (21)	0.591 7 (3)
C(a4)	0.1927 (3)	0.199 94 (19)	0.147 91 (27)	C(46)	−0.0951 (4)	0.151 20 (20)	0.518 28 (28)
C(a5)	0.1069 (3)	0.124 93 (19)	0.096 39 (25)	C(47)	0.0839 (3)	0.053 86 (21)	0.487 20 (29)
C(a6)	−0.0198 (3)	0.091 93 (19)	0.120 66 (26)	C(48)	−0.0585 (4)	0.095 11 (23)	0.714 5 (3)
C(a7)	−0.0939 (3)	0.088 70 (19)	0.232 30 (27)	C(49)	−0.1542 (4)	0.191 45 (24)	0.476 2 (3)
C(a8)	−0.0508 (3)	0.112 03 (19)	0.348 23 (26)	C(51)	−0.1046 (3)	0.221 63 (20)	0.238 37 (27)
C(b1)	0.0697 (3)	0.219 49 (20)	0.461 73 (26)	C(52)	−0.1728 (3)	0.254 47 (20)	0.212 50 (28)
C(b2)	0.1123 (3)	0.258 13 (20)	0.431 85 (27)	C(53)	−0.1708 (3)	0.281 30 (20)	0.145 66 (28)
C(b3)	0.2438 (3)	0.275 47 (20)	0.196 34 (28)	C(54)	−0.0964 (3)	0.272 54 (20)	0.109 20 (28)
C(b4)	0.2514 (3)	0.242 30 (20)	0.140 45 (27)	C(55)	−0.0315 (3)	0.238 53 (19)	0.139 48 (27)
C(b5)	0.0774 (3)	0.089 35 (19)	0.038 36 (26)	C(56)	−0.3133 (4)	0.321 14 (22)	0.155 0 (3)
C(b6)	−0.0021 (3)	0.070 43 (19)	0.052 06 (26)	C(57)	−0.2290 (4)	0.343 31 (22)	0.049 9 (3)
C(b7)	−0.1535 (3)	0.065 39 (20)	0.277 32 (27)	C(58)	0.2284 (3)	0.125 84 (20)	0.327 60 (28)
C(b8)	−0.1252 (3)	0.077 77 (20)	0.348 04 (27)	C(59)	0.2873 (3)	0.091 46 (21)	0.363 98 (27)
C(m1)	0.1642 (3)	0.272 61 (19)	0.307 94 (26)	C(60)	0.2692 (3)	0.037 75 (20)	0.360 32 (27)
C(m2)	0.1770 (3)	0.159 45 (20)	0.096 61 (26)	C(61)	0.1908 (3)	0.023 19 (20)	0.314 61 (29)
C(m3)	−0.0920 (3)	0.079 35 (18)	0.157 56 (26)	C(62)	0.1365 (3)	0.060 38 (20)	0.279 95 (27)
C(m4)	−0.0109 (3)	0.139 06 (19)	0.408 82 (26)	C(63)	0.4041 (4)	0.016 87 (23)	0.443 6 (3)
C(11)	0.2041 (3)	0.324 51 (18)	0.330 03 (26)	C(64)	0.2964 (4)	−0.052 76 (24)	0.396 1 (4)
C(12)	0.1627 (3)	0.369 55 (20)	0.300 16 (26)	Cl(1)	−0.46280 (10)	0.145 52 (6)	−0.503 81 (8)
C(13)	0.2035 (3)	0.417 44 (19)	0.316 45 (27)	O(1)	−0.41506 (29)	0.114 15 (17)	−0.550 18 (22)
C(14)	0.2842 (3)	0.421 26 (20)	0.359 79 (27)	O(2)	−0.53370 (28)	0.172 93 (17)	−0.548 25 (22)
C(15)	0.3257 (3)	0.375 94 (21)	0.387 53 (27)	O(3)	−0.49942 (26)	0.113 44 (15)	−0.451 12 (22)
C(16)	0.2874 (3)	0.327 38 (19)	0.374 01 (26)	O(4)	−0.40361 (28)	0.181 96 (17)	−0.464 12 (24)
C(17)	0.0774 (3)	0.366 78 (21)	0.248 07 (28)	Cl(2)	0.47306 (12)	0.031 51 (8)	0.253 59 (10)
C(18)	0.3272 (4)	0.473 11 (21)	0.378 64 (29)	C(65)	0.5748 (4)	0.000 50 (26)	0.279 6 (4)
C(19)	0.3353 (3)	0.279 07 (21)	0.404 04 (29)	C(66)	0.6173 (4)	0.009 93 (26)	0.350 2 (4)
C(21)	0.2363 (3)	0.156 90 (19)	0.036 99 (26)	C(67)	0.6976 (4)	−0.016 00 (28)	0.372 4 (4)
C(22)	0.2077 (3)	0.174 78 (20)	−0.034 70 (27)	C(68)	0.7323 (4)	−0.046 75 (27)	0.324 5 (5)
C(23)	0.2681 (3)	0.174 18 (20)	−0.086 62 (27)	C(69)	0.6879 (5)	−0.054 02 (27)	0.252 3 (4)
C(24)	0.3547 (3)	0.157 53 (20)	−0.068 25 (28)	C(70)	0.6091 (5)	−0.029 16 (28)	0.228 9 (4)
C(25)	0.3810 (3)	0.141 05 (20)	0.003 59 (28)	Cl(3)	−0.02185 (14)	0.228 69 (9)	−0.247 65 (12)
C(26)	0.3239 (3)	0.139 98 (19)	0.056 63 (28)	C(71)	0.0368 (5)	0.282 93 (29)	−0.267 0 (4)
C(27)	0.1157 (4)	0.196 92 (22)	−0.056 95 (29)	C(72)	0.0422 (5)	0.296 09 (29)	−0.343 6 (4)
C(28)	0.4196 (4)	0.159 26 (23)	−0.123 7 (3)	C(73)	0.0903 (5)	0.338 2 (3)	−0.360 1 (5)
C(29)	0.3557 (3)	0.121 09 (22)	0.134 58 (29)	C(74)	0.1323 (6)	0.370 0 (4)	−0.303 2 (6)
C(31)	−0.1707 (3)	0.055 96 (19)	0.110 18 (26)	C(75)	0.1284 (7)	0.355 4 (4)	−0.226 7 (6)
C(32)	−0.2273 (3)	0.090 15 (20)	0.068 18 (26)	C(76)	0.0779 (6)	0.312 8 (3)	−0.208 3 (5)

[a] The estimated standard deviations of the least significant digits are given in parentheses.

The Mössbauer spectrum may then be described in terms of the nuclear Hamiltonian

$$\mathcal{H}_N = \vec{S}\cdot\vec{A}\cdot\vec{I} + (QV_{zz}/4)\{I_z^2 - I(I+1)/3 + (\eta/3)(I_x^2 - I_y^2)\} - g_N\beta_N\vec{H}\cdot\vec{I} \quad (4)$$

Using the program of Lang and Dale,[79] the 4.2 K, 6-T spectrum was fit by adjusting the asymmetry parameter η and the hyperfine coupling constants A_x, A_y, and A_z, which in turn, through eqs 1–3 determine the g and A values. The quadrupole splitting (ΔE_q), isomer shift (δ), and line width were set at values found in zero field, while the values of κ and P were set to 0.35 and −4.2 mm/s, respectively,[78] for the fitting procedure. From the best fit values of η, Δ/λ, and V/λ the values of a, b, and c and the g and A values were calculated. The values of η and $QV_{zz}/4$ can also be estimated from the expressions given by Lang and Marshall,[76] expressed in the Taylor formalism:

$$QV_{zz}/4 = (a^2/2 + b^2/2 - c^2)(1.5 \text{ mm/s}) \quad (5)$$

$$\eta = -3/2(a^2 - b^2)/(a^2/2 + b^2/2 - c^2) \quad (6)$$

Since, for these large g_{max} species, the factors that affect the total magnetic splitting are dominated by the largest g and A values, there is less sensitivity than desired in the dependence of the fit on the values of A_x and A_y and g_x and g_y. A considerably better fit was achieved by rotating the axes of the **g** and **A** tensors by 45° in counterclockwise directions. Figure 2a shows the fit for $\Delta/\lambda = 1.9$ and $V/\lambda = 0.7$, which gave the g and A values presented in the first column of Table VII. This set of g values yields $\sum g^2 = 15.2$, slightly less than the suggested $\sum g^2 = 16$ relationship of Griffith.[74] (However, it should be noted that the EPR parameters of $[Fe(TPP)(Py)_2]Cl$, obtained from single-crystal EPR investigations[59] (Table V), also yield $\sum g^2 = 15.2$. On the other hand, this set of g values also leads to $a^2 + b^2 + c^2 = 1.0192$, a considerably greater deviation from the expected 1.0000 than the data shown in Table VII.) As an alternative means of fitting the Mössbauer spectra, one might assume $\sum g^2 = 15.8$ and $\Delta/\lambda = 3.6$ (as found for other bis[4-(dimethylamino)pyridine] complexes of iron(III) porphyrinates, all of which give normal rhombic EPR spectra, Table V). Using this additional constraint to simulate the Mössbauer spectrum yields a similar, acceptable fit to the data. The resulting parameters are listed in the second column of Table VII. In this case, $V/\lambda = 0.89$, only slightly larger than for the first fit.

Figure 2b shows the magnetic Mössbauer spectrum of $[Fe(OEP)(4\text{-}NMe_2Py)_2]ClO_4$ at 4.2 K (6 T). In comparison to the well-resolved doublet observed at 77 K (Figure 1b), the spectrum

Table IV. Fractional Coordinates for $[Fe(TMP)(1\text{-}MeIm)_2]ClO_4$[a]

atom	x	y	z	atom	x	y	z
Fe(1)	0.0000	0.0000	0.0000	C(22)	−0.09350 (23)	−0.39506 (23)	0.01264 (23)
Fe(2)	0.5000	0.5000	0.5000	C(23)	−0.12253 (25)	−0.48475 (23)	0.03093 (25)
N(1)	0.12555 (18)	0.08642 (17)	0.01712 (17)	C(24)	−0.14374 (26)	−0.50182 (25)	0.11205 (28)
N(2)	0.08022 (18)	−0.09576 (18)	0.06501 (17)	C(25)	−0.13334 (27)	−0.42654 (27)	0.17680 (26)
N(3)	0.01140 (20)	−0.05327 (18)	−0.11995 (18)	C(26)	−0.10268 (26)	−0.33556 (25)	0.16292 (24)
N(4)	0.02732 (23)	−0.06086 (22)	−0.25986 (20)	C(27)	−0.07449 (29)	−0.38020 (25)	−0.07868 (26)
N(5)	0.38961 (18)	0.42794 (17)	0.39543 (17)	C(28)	−0.1796 (3)	−0.60023 (28)	0.1287 (3)
N(6)	0.40633 (18)	0.49341 (17)	0.57723 (17)	C(29)	−0.0921 (4)	−0.2565 (3)	0.23625 (28)
N(7)	0.54413 (20)	0.38120 (18)	0.54121 (19)	C(31)	0.14219 (24)	0.36850 (24)	0.45214 (22)
N(8)	0.54075 (26)	0.23581 (21)	0.57373 (25)	C(32)	0.06699 (26)	0.41994 (26)	0.40570 (24)
C(a1)	0.13511 (24)	0.17422 (22)	−0.01206 (22)	C(33)	−0.03275 (27)	0.3890 (3)	0.39900 (28)
C(a2)	0.22326 (23)	0.06853 (22)	0.05741 (22)	C(34)	−0.06088 (28)	0.3101 (3)	0.43581 (28)
C(a3)	0.18383 (25)	−0.08794 (23)	0.10094 (23)	C(35)	0.01429 (28)	0.26051 (26)	0.48191 (26)
C(a4)	0.04423 (24)	−0.18384 (22)	0.08235 (22)	C(36)	0.11573 (26)	0.28767 (25)	0.48970 (24)
C(a5)	0.39632 (24)	0.40046 (22)	0.30841 (22)	C(37)	0.0918 (3)	0.5086 (3)	0.3658 (3)
C(a6)	0.29336 (23)	0.39105 (22)	0.39483 (22)	C(38)	−0.1711 (3)	0.2790 (4)	0.4275 (4)
C(a7)	0.30644 (23)	0.45302 (22)	0.55188 (22)	C(39)	0.19443 (29)	0.22936 (27)	0.5386 (3)
C(a8)	0.42995 (23)	0.52641 (22)	0.66963 (22)	C(41)	0.53595 (23)	0.59846 (23)	0.82595 (22)
C(b1)	0.23971 (25)	0.21077 (23)	0.01092 (24)	C(42)	0.59188 (24)	0.54395 (23)	0.88984 (23)
C(b2)	0.29332 (24)	0.14621 (24)	0.05249 (24)	C(43)	0.60530 (25)	0.56559 (26)	0.98376 (24)
C(b3)	0.21197 (26)	−0.17138 (26)	0.14100 (27)	C(44)	0.56482 (26)	0.63886 (26)	1.01587 (23)
C(b4)	0.12681 (27)	−0.22991 (24)	0.12949 (25)	C(45)	0.50762 (26)	0.68990 (24)	0.95161 (24)
C(b5)	0.30511 (26)	0.34301 (25)	0.25480 (23)	C(46)	0.49237 (24)	0.67185 (23)	0.85654 (23)
C(b6)	0.24197 (25)	0.33698 (25)	0.30734 (24)	C(47)	0.63845 (29)	0.46297 (27)	0.85819 (27)
C(b7)	0.26826 (24)	0.46316 (24)	0.62928 (23)	C(48)	0.5866 (3)	0.6656 (3)	1.11895 (26)
C(b8)	0.34431 (25)	0.50606 (24)	0.70191 (22)	C(49)	0.4333 (3)	0.73318 (26)	0.79015 (26)
C(m1)	0.25186 (23)	−0.01184 (23)	0.09693 (23)	C(1)	0.0082 (3)	−0.00940 (26)	−0.19356 (26)
C(m2)	−0.05642 (24)	−0.22192 (22)	0.05779 (22)	C(2)	0.0352 (4)	−0.1385 (3)	−0.1421 (3)
C(m3)	0.25146 (23)	0.40478 (22)	0.46595 (22)	C(3)	0.0433 (4)	−0.1436 (3)	−0.2287 (3)
C(m4)	0.52242 (24)	0.57494 (22)	0.72424 (22)	C(4)	0.0328 (4)	−0.0327 (3)	−0.35014 (28)
C(11)	0.36307 (25)	−0.01858 (23)	0.13328 (26)	C(5)	0.4888 (3)	0.3045 (3)	0.5449 (4)
C(12)	0.41982 (28)	0.02253 (26)	0.22250 (26)	C(6)	0.6386 (3)	0.3590 (3)	0.5741 (5)
C(13)	0.5239 (3)	0.0149 (3)	0.2529 (3)	C(7)	0.6362 (4)	0.2699 (3)	0.5926 (4)
C(14)	0.5696 (3)	−0.0316 (3)	0.1982 (4)	C(8)	0.5027 (4)	0.1409 (4)	0.5862 (5)
C(15)	0.5127 (3)	−0.0701 (3)	0.1108 (4)	Cl	0.22159 (13)	−0.04656 (11)	0.45052 (12)
C(16)	0.40965 (28)	−0.06451 (26)	0.07714 (29)	O(1)	0.1626 (4)	−0.0422 (3)	0.5098 (3)
C(17)	0.3733 (3)	0.0752 (4)	0.28388 (29)	O(2)	0.2227 (5)	0.0403 (3)	0.4135 (5)
C(18)	0.6823 (3)	−0.0390 (4)	0.2340 (4)	O(3)	0.1833 (5)	−0.1159 (4)	0.3815 (4)
C(19)	0.3501 (3)	−0.1085 (3)	−0.0195 (3)	O(4)	0.3175 (4)	−0.0634 (4)	0.4967 (4)
C(21)	−0.08430 (23)	−0.31967 (22)	0.07866 (23)				

[a] The estimated standard deviations of the least significant digits are given in parentheses.

at 4.2 K is poorly resolved, even in applied field. Such poorly resolved hyperfine spectra are typical of low-spin iron(III) porphyrinates.[41,80] An approximate fit to the magnetic spectrum, setting $P = -4.2$ mm/s and $\kappa = 0.35$, gives $\Delta/\lambda = 3.2$ and $V/\lambda = 2.0$, $\eta = 1.83$. The calculated g values are close to the values determined by EPR spectroscopy (Table VII). Again, as discussed by Oosterhuis and Lang,[75] it is necessary to rotate the g and hyperfine axes by 45° in opposite directions about the heme normal so that the direction of g_x coincides with A_y and g_y coincides with A_x. The relationship derived by Bohan[81] from the Griffith theorem for $k = 1$

$$g_x^2 + g_y^2 + g_z^2 - g_xg_y - g_xg_z + g_yg_z + 4g_x - 4g_y - 4g_z = 0 \quad (7)$$

is obeyed for the g values derived from the Mössbauer spectra of both complexes.

The Mössbauer spectrum of $[Fe(TMP)(1\text{-}MeIm)_2]ClO_4$ at 77 K is shown in Figure 1c. The isomer shift and quadrupole splitting constant obtained from the 77 K spectrum are listed in Table VI. These values of isomer shift and quadrupole splitting are temperature independent within experimental error. Because of the broadening at low temperature, a spectrum of this complex with applied magnetic field was not attempted.

The molecular structures of the three complexes are shown in the ORTEP diagrams for $[Fe(TMP)(4\text{-}NMe_2Py)_2]ClO_4$ (Figure 3), $[Fe(OEP)(4\text{-}NMe_2Py)_2]ClO_4$ (Figure 4), and the two independent half-molecules of $[Fe(TMP)(1\text{-}MeIm)_2]ClO_4$ (Figure 5). The numbering schemes for the crystallographically unique atoms and bond distances in each coordination group are also displayed in these figures. $[Fe(TMP)(4\text{-}NMe_2Py)_2]ClO_4$ has its two pyridine ligands arranged in nearly perpendicular orientation from each other. The ligand planes make dihedral angles ϕ of 37° and 42° to the closest Fe–N_p axis. This results in a relative ligand plane orientation of 79° compared to the 90° nominal value for

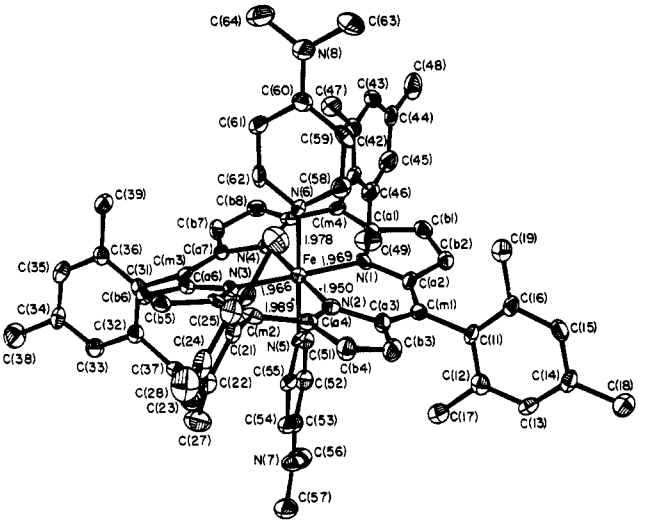

Figure 3. ORTEP diagram of $[Fe(TMP)(4\text{-}NMe_2Py)_2]ClO_4$. Labels assigned to the crystallographically unique molecule are displayed. 60% probability surfaces are shown.

(80) Walker, F. A.; Parak, F. Unpublished data.
(81) Bohan, T. *J. Magn. Reson.* **1977**, *26*, 109–18.
(82) Yoshimura, T.; Ozaki, T. *Arch. Biochem. Biophys.* **1984**, *230*, 466–82.
(83) Peisach, J.; Mims, W. B. *Biochemistry* **1977**, *16*, 2795–99.

Table V. EPR Spectra of Bis-Ligated Pyridine and Imidazole Porphinatoiron(III) Derivatives

complex	ligand $pK_a(BH^+)$[a]	T, K	medium	g_1	g_2	g_3	ref
			Pyridine Derivatives				
$[Fe(OEP)(4\text{-}NMe_2Py)_2]ClO_4$	9.70	25	crystalline	2.818[b]	2.275[b]	1.630[b]	this work
		25	CH_2Cl_2	2.818[b]	2.278[b]	1.642[b]	this work
$[Fe(TMP)(4\text{-}NMe_2Py)_2]ClO_4$	9.70	17	crystalline	3.48			this work
		24	CH_2Cl_2	3.33			this work
$[Fe(T2,6\text{-}Cl_2PP)(4\text{-}NMe_2Py)_2]ClO_4$	9.70	77	crystalline	2.70	2.30	1.70	this work
		24	CH_2Cl_2	3.54			this work
$[Fe(TPP)(4\text{-}NMe_2Py)_2]I$	9.70	77	CH_2Cl_2	2.786	2.284	1.657	38
$[Fe(T2,6\text{-}Cl_2PP)(4\text{-}NH_2Py)_2]ClO_4$	9.29	77	crystalline	2.76	2.27	1.70	this work
		24	CH_2Cl_2	3.24			this work
$[Fe(TPP)(4\text{-}NH_2Py)_2]I$	9.29	77	CH_2Cl_2	2.830	2.289	1.603	38
$[Fe(TPP)(3,4\text{-}(NH_2)_2Py)_2]I$	9.14	77	CH_2Cl_2	2.864	2.280	1.597	38
$[Fe(TPP)(3\text{-}Me,4\text{-}NMe_2Py)_2]I$	8.69	77	CH_2Cl_2	2.865	2.286	1.591	38
$[Fe(TPP)(3,5\text{-}Me_2,4\text{-}NMe_2Py)_2]I$	8.12	77	CH_2Cl_2	2.785	2.281	1.675	38
$[Fe(TPP)(3,4\text{-}Me_2Py)_2]I$	6.46	<30	CH_2Cl_2	3.4			38
$[Fe(TPP)(2\text{-}Quin)_2]I$	5.40	<30	CH_2Cl_2	3.44			38
$[Fe(TPP)(Py)_2]ClO_4$	5.20	6	single-crystal	3.7	1.12	−0.46	59
			Imidazole Derivatives				
$[Fe(TMP)(1\text{-}MeIm)_2]ClO_4$[c,d]	7.33	25	CH_2Cl_2	2.886[b]	2.325[b]	1.571[b]	this work
$[Fe(TPP)(HIm)_2]Cl\cdot CHCl_3\cdot H_2O$[c,e]	6.65	6	crystalline	2.84	2.32	1.59	66
				3.00	2.2	1.47	
$[Fe(TPP)(1\text{-}MeIm)_2]ClO_4$	7.33	77	crystalline	2.866	2.276	1.535	67
		77	CH_2Cl_2	2.890	2.291	1.554	67
$[Fe(TPP)(1\text{-}MeIm)_2]I$	7.33	77	CH_2Cl_2	2.886	2.294	1.549	38
$[Fe(TPP)(1\text{-}BzlIm)_2]I$	7.0	77	CH_2Cl_2	2.860	2.306	1.561	38
$[Fe(TPP)(4\text{-}MeHIm)_2]I$	7.22	77	CH_2Cl_2	2.847	2.288	1.590	38
$[Fe(TPP)(4\text{-}PhHIm)_2]I$	5.70	77	CH_2Cl_2	2.893	2.307	1.552	38
$[Fe(TPP)(c\text{-}MU)_2]SbF_6$[c,e]		77	single crystal	2.999	2.265	1.481	68
				2.965	2.298	1.486	
$[Fe(TPP)(t\text{-}MU)_2]SbF_6$		77	single crystal	2.964	2.269	1.471	68
$[K(K222)][Fe(TPP)(4\text{-}MeIm)_2]$	7.22	77	crystalline	2.60	2.24	1.82	69
		77	CH_2Cl_2	2.60	2.24	1.82	69
$[Fe(TPP)(2\text{-}MeHIm)_2]Cl$	7.56	11	crystalline	3.56			41
		6	DMF	3.41			41
$[Fe(TPP)(2\text{-}MeHIm)_2]I$	7.56	<30	CH_2Cl_2	3.40			38
$[Fe(TPP)(5,6\text{-}Me_2BzHIm)_2]I$	5.68	<30	CH_2Cl_2	3.43			38
$[Fe(TPP)(1,2\text{-}Me_2Im)_2]I$	7.85	<30	CH_2Cl_2	3.40			38

[a] pK_a values obtained from ref 42. [b] Footnoted g values ±0.005; others of this study to ±0.01. [c] Structure consists of two independent half-molecules in the asymmetric unit cell. [d] Overlapping EPR signals obtained in the solid state; assignment not possible. [e] Two overlapping EPR signals obtained in the solid state.

Table VI. Mössbauer Parameters[a] and Calculated Crystal Field Values of Bis-Ligated Pyridine and Imidazole Porphinatoiron(III) Derivatives

complex	medium[b]	T, K (appl field, T)	δ, mm s^{-1}	ΔE, mm s^{-1}	lw, mm s^{-1}		V/λ	Δ/λ	ref
			Pyridine Derivatives						
$[Fe(TMP)(4\text{-}NMe_2Py)_2]ClO_4$	crystalline	77	0.20	1.74	0.43	0.94			
		4.2 (6)	0.18	1.75	0.32		0.4	1.8	this work
$[Fe(OEP)(4\text{-}NMe_2Py)_2]ClO_4$	crystalline	77	0.26	2.14	0.28	0.37			
		4.2 (6)	0.26	2.15	0.29		2.0	3.2	this work
$[Fe(TPP)(Py)_2]Cl$	solid[c]	77	0.16	1.25					70
$[Fe(Proto\ IX)(Py)_2]Cl$	solid	77	0.23	1.88					70
$[Fe(Proto\ IX)(Py)_2]Cl$	H_2O/pyridine	4.2	0.28	1.95			0.8	1.4	71
			Imidazole Derivatives						
$[Fe(TMP)(1\text{-}MeIm)_2]ClO_4$	crystalline	77	0.28	2.28	0.71	0.94			
		4.2 (0)	0.28	2.31	0.78	0.96			this work
$[Fe(TPP)(2\text{-}MeHIm)_2]Cl$	crystalline	150	0.22	1.77					63
$[Fe(TPP)(HIm)_2]Cl$	crystalline(?)	77	0.23	2.23					70
		298	0.13	2.11					70
$[Fe(Proto\ IX)(HIm)_2]Cl$	solid[d]	77	0.24	2.30					70
		298	0.14	2.17					
$[Fe(Proto\ IX\ DME)(HIm)_2]Cl$	solid[d]	77	0.24	2.35					70
		298	0.15	2.21					
$[Fe(Tp\text{-}OCH_3PP)(HIm)_2]Cl$	solid	298	0.17	2.06					73
$[Fe(Tp\text{-}ClPP)(HIm)_2]Cl$	solid	298	0.15	2.01					73
$[Fe(Proto\ IX)(1\text{-}MeIm)_2]Cl$	DMSO	80	0.23	2.24	0.37	0.49			72
$[Fe(Proto\ IX)(HIm)_2]Cl$	DMSO	80	0.22	2.38	0.21	0.26			72
$[Fe(Proto\ IX)(HIm)(Im)]$	DMSO + NBu_4OH	80	0.24	2.43	0.27	0.25			72
$[Fe(Proto\ IX)(2\text{-}MeHIm)_2]Cl$	H_2O + ethanol	80	0.16	1.87	0.29	0.59			72
$[Fe(TPP)(2\text{-}MeHIm)_2]Cl$	DMF	150	0.21	1.71			0.88	2.96	63
Cytochrome b_5	H_2O(?)	195	0.23	2.27					82

[a] All values relative to metallic iron. [b] Crystalline indicates that X-ray structure and Mössbauer measured on the same crystalline phase, while the (?) indicates some uncertainty about the phase used for the Mössbauer study. [c] Structure of closely related species known to have perpendicular ligands. [d] Structure of closely related species known to have parallel ligands.

Table VII. Crystal Field and Hyperfine Parameters Calculated from the Mössbauer Spectra of the Bis[4-(Dimethylamino)pyridine] Complexes of This Study[a]

	[Fe(TMP)(4-NMe$_2$Py)$_2$]-ClO$_4$			[Fe(OEP)-(4-NMe$_2$Py)$_2$]ClO$_4$	
	calcd		exptl	calcd	exptl
Δ/λ	1.9[b]	3.6[c]		3.2	
V/λ	0.7[b]	0.89[c]		2.2	
V/Δ	0.37[b]	0.25[c]		0.69	
g_x	0.36[b]	0.92[c]		1.58	1.63
g_y	1.91[b]	1.80[c]		2.30	2.28
g_z	3.38[b]	3.44[c]	3.48	2.83	2.82
Σg^2	15.20	15.92		15.80	15.81
ΔE_Q, mm/s	1.75	1.75	1.75	2.15	2.15
$A_x/g_N\mu_N$, kG	−362[b]	−331[c]		−416	
$A_y/g_N\mu_N$, kG	338[b]	168[c]		177	
$A_z/g_N\mu_N$, kG	812[b]	815[c]		446	
QV_{zz}, mm/s	2.46[b]	2.80[c]		2.84	
η	−1.75[b]	−1.96[c]	−1.00	−2.77	−1.83
$a^2 + b^2 + c^2$	1.0016[b]	1.0006[c]		0.9999	
χ^2[d]	340[d]	392[d]		394[d]	

[a] Simulations done setting $P = -4.2$ mm/s, $\kappa = 0.35$. [b] Parameters obtained from the unconstrained fit (see text). [c] Parameters obtained from the fit in which Δ/λ was set to 3.6. [d] Goodness-of-fit parameter (relative).

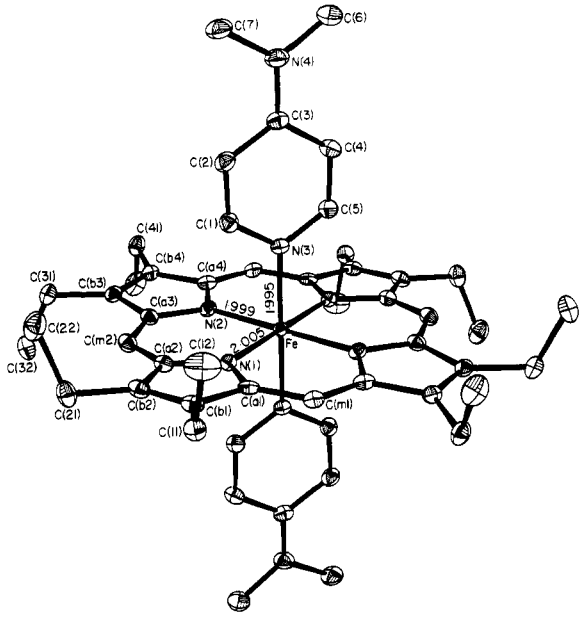

Figure 4. ORTEP diagram of [Fe(OEP)(4-NMe$_2$Py)$_2$]ClO$_4$. Labels assigned to the crystallographically unique atoms of the centrosymmetric molecule are displayed. 60% probability surfaces are shown.

a "perpendicular" orientation. [Fe(OEP)(4-NMe$_2$Py)$_2$]ClO$_4$ has crystallographically required inversion symmetry at iron, and thus the two pyridine ligand planes are coplanar with a unique ϕ angle of 36°. The crystal structure of [Fe(TMP)(1-MeIm)$_2$]ClO$_4$ consists of two independent half-molecules, molecules 1 and 2, in the asymmetric unit of structure. The two iron atoms are each at an inversion center; hence, the two imidazoles of each molecule have relative parallel orientations. The dihedral angle ϕ for molecule 1 is 23° and that for molecule 2 is 42°. The axial ligands in [Fe(OEP)(4-NMe$_2$Py)$_2$]ClO$_4$ are effectively perpendicular to the porphyrin plane, while the other complexes display significant deviation from exact perpendicularity. The imidazole planes in [Fe(TMP)(1-MeIm)$_2$]ClO$_4$ form dihedral angles of 83.7° (molecule 1) and 88.8° (molecule 2). Such deviations have been commonly noted for imidazole derivatives coordinated to metalloporphyrins.[84] Although pyridine ligand planes are normally

(84) Momenteau, M.; Scheidt, W. R.; Eigenbrot, C. W.; Reed, C. A. *J. Am. Chem. Soc.* **1988**, *110*, 1207-15.

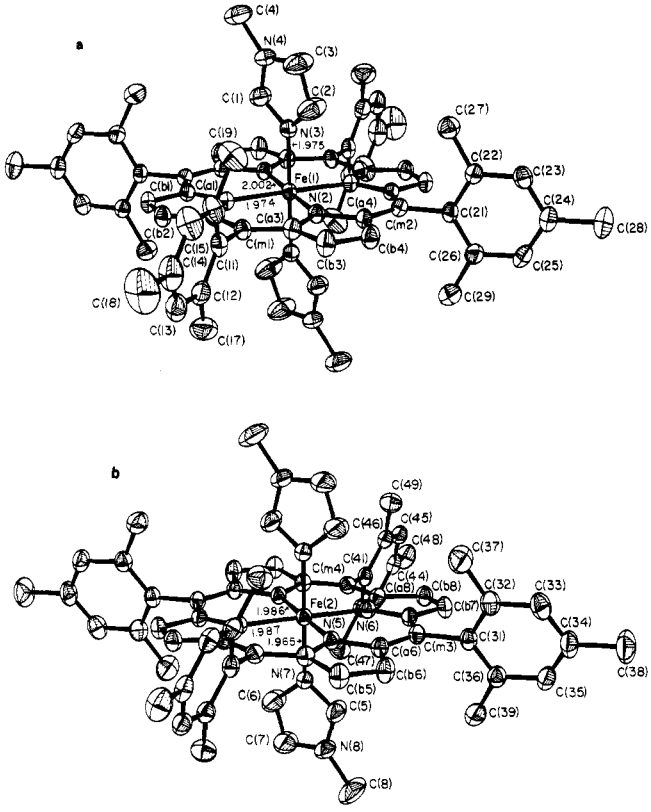

Figure 5. ORTEP diagram of [Fe(TMP)(1-MeIm)$_2$]ClO$_4$: (a) molecule 1; (b) molecule 2. The same information is given as in Figure 4. 25% probability surfaces are shown.

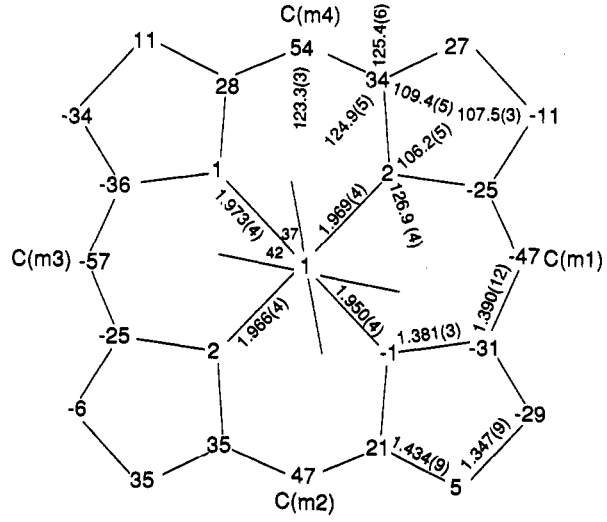

Figure 6. Formal diagram of the porphinato core in [Fe(TMP)(4-NMe$_2$Py)$_2$]ClO$_4$. Deviations of each unique atom from the mean plane of the core (in units of 0.01 Å) are shown. Averaged values for the chemically unique bond distances and angles in the core are shown. The numbers in parentheses following each averaged value are the estimated standard deviations calculated on the assumption that all values are drawn from the same population. The orientations of the axial ligands with the closest Fe–N$_p$ vector (angle ρ) are shown. Individual values of the Fe–N$_p$ bond distances are shown.

orthogonal to the porphyrin core, the dihedral angles between the pyridine planes and the core in [Fe(TMP)(4-NMe$_2$Py)$_2$]ClO$_4$ show substantial deviation; the observed angles are 88.3 and 82.4°.

Averaged values for the chemically equivalent bond distances and angles in the cores of the three complexes are shown in Figures 6–8. The number in parentheses following each averaged value is the estimated standard deviation calculated on the assumption that the individual values are all drawn from the same population. Individual values of the Fe–N$_p$ bond distances and their rela-

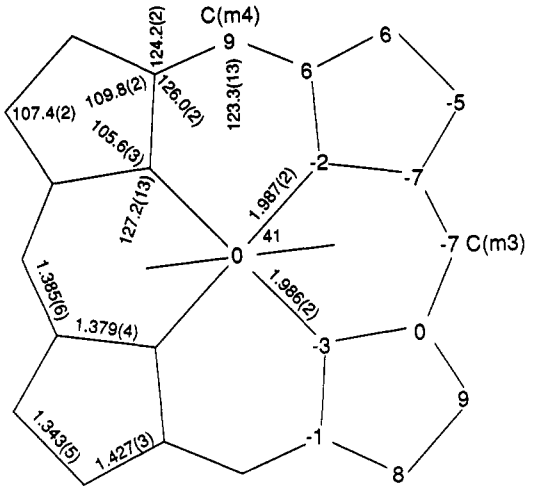

Figure 7. Formal diagram of the porphinato core in $[Fe(OEP)(4\text{-}NMe_2Py)_2]ClO_4$. Deviations of each unique atom from the mean plane of the core (in units of 0.01 Å) are shown. Values for the centrosymmetrically related atoms have the same magnitude displacement but opposite sign. The same information displayed in Figure 6 is given.

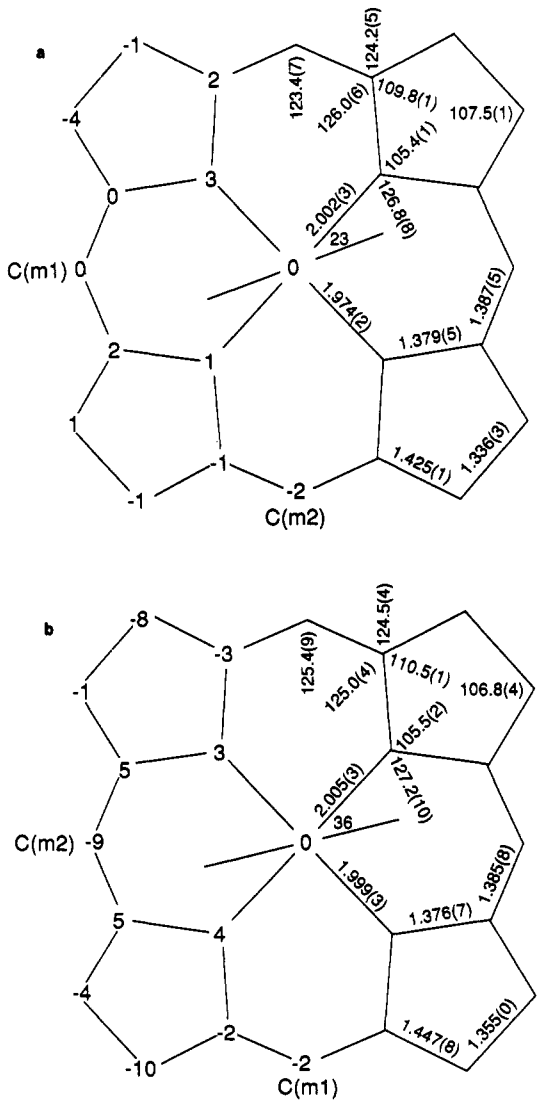

Figure 8. Formal diagram of the porphinato core in $[Fe(TMP)(1\text{-}MeIm)_2]ClO_4$: (a) molecule 1; (b) molecule 2. The same information displayed in Figures 6 and 7 is given in this figure.

tionship to the axial ligand orientations are also shown in the diagrams. The two independent axial bond distances in $[Fe(TMP)(4\text{-}NMe_2Py)_2]ClO_4$ are 1.989 (4) and 1.978 (4) Å while the distance in $[Fe(OEP)(4\text{-}NMe_2Py)_2]ClO_4$ is 1.995 (3) Å. As has been generally observed,[85] the axial metal–imidazole distances are somewhat shorter than the pyridine values with distances of 1.975 (3) Å in molecule 1 and 1.965 (3) Å in molecule 2 of $[Fe(TMP)(1\text{-}MeIm)_2]ClO_4$. Individual bond distances and angles for $[Fe(TMP)(4\text{-}NMe_2Py)_2]ClO_4$ are given in Tables VIII and IX while complete values of individual bond distances and angles for $[Fe(TMP)(1\text{-}MeIm)_2]ClO_4$ and $[Fe(OEP)(4\text{-}NMe_2Py)_2]ClO_4$ are given in Tables SIX–SXII.

Figures 6–8 are formal diagrams showing the displacements of the crystallographically unique atoms from the mean plane of the 24-atom core (in units of 0.01 Å). $[Fe(TMP)(4\text{-}NMe_2Py)_2]ClO_4$ has a significantly S_4-ruffled core while [Fe-

Table VIII. Bond Distances in $[Fe(TMP)(4\text{-}NMe_2Py)_2]ClO_4\cdot 2C_6H_5Cl$[a]

type	length, Å	type	length, Å
Fe–N(1)	1.969 (4)	C(24)–C(25)	1.381 (7)
Fe–N(2)	1.950 (4)	C(24)–C(28)	1.505 (7)
Fe–N(3)	1.966 (4)	C(25)–C(26)	1.384 (7)
Fe–N(4)	1.973 (4)	C(26)–C(21)	1.404 (7)
Fe–N(5)	1.989 (4)	C(26)–C(29)	1.516 (7)
Fe–N(6)	1.978 (4)	C(31)–C(32)	1.388 (7)
N(1)–C(a1)	1.379 (6)	C(32)–C(33)	1.389 (7)
N(1)–C(a2)	1.380 (6)	C(32)–C(37)	1.516 (7)
N(2)–C(a3)	1.386 (6)	C(33)–C(34)	1.380 (7)
N(2)–C(a4)	1.381 (6)	C(34)–C(35)	1.396 (7)
N(3)–C(a5)	1.386 (6)	C(34)–C(38)	1.513 (7)
N(3)–C(a6)	1.383 (6)	C(35)–C(36)	1.388 (7)
N(4)–C(a7)	1.379 (6)	C(36)–C(31)	1.402 (7)
N(4)–C(a8)	1.377 (6)	C(36)–C(39)	1.518 (7)
N(5)–C(51)	1.346 (4)	C(41)–C(42)	1.401 (7)
N(5)–C(55)	1.351 (4)	C(42)–C(43)	1.397 (7)
N(6)–C(58)	1.367 (4)	C(42)–C(47)	1.504 (7)
N(6)–C(62)	1.348 (4)	C(43)–C(44)	1.389 (7)
C(a1)–C(b1)	1.448 (7)	C(44)–C(45)	1.383 (7)
C(a1)–C(m4)	1.400 (7)	C(44)–C(48)	1.513 (7)
C(a2)–C(b2)	1.428 (6)	C(45)–C(46)	1.390 (7)
C(a2)–C(m1)	1.396 (6)	C(46)–C(41)	1.406 (7)
C(a3)–C(b3)	1.446 (7)	C(46)–C(49)	1.514 (7)
C(a3)–C(m1)	1.372 (6)	C(51)–C(52)	1.374 (7)
C(a4)–C(b4)	1.431 (7)	C(52)–C(53)	1.403 (7)
C(a4)–C(m2)	1.400 (7)	C(53)–N(7)	1.360 (6)
C(a5)–C(b5)	1.425 (6)	C(53)–C(54)	1.406 (7)
C(a5)–C(m2)	1.391 (7)	C(54)–C(55)	1.381 (7)
C(a6)–C(b6)	1.424 (6)	N(7)–C(56)	1.457 (7)
C(a6)–C(m3)	1.401 (6)	N(7)–C(57)	1.444 (7)
C(a7)–C(b7)	1.434 (6)	C(58)–C(59)	1.368 (7)
C(a7)–C(m3)	1.384 (6)	C(59)–C(60)	1.413 (7)
C(a8)–C(b8)	1.437 (7)	C(60)–N(8)	1.347 (6)
C(a8)–C(m4)	1.375 (7)	C(60)–C(61)	1.412 (7)
C(b1)–C(b2)	1.344 (7)	C(61)–C(62)	1.365 (7)
C(b3)–C(b4)	1.346 (7)	N(8)–C(63)	1.459 (6)
C(b5)–C(b6)	1.359 (6)	N(8)–C(64)	1.466 (7)
C(b7)–C(b8)	1.339 (7)	Cl(1)–O(1)	1.435 (4)
C(m1)–C(11)	1.503 (6)	Cl(1)–O(2)	1.444 (4)
C(m2)–C(21)	1.503 (6)	Cl(1)–O(3)	1.435 (4)
C(m3)–C(31)	1.506 (6)	Cl(1)–O(4)	1.429 (4)
C(m4)–C(41)	1.492 (6)	Cl(2)–C(65)	1.752 (7)
C(11)–C(12)	1.397 (7)	C(65)–C(66)	1.381 (8)
C(12)–C(13)	1.397 (7)	C(66)–C(67)	1.405 (8)
C(12)–C(17)	1.504 (7)	C(67)–C(68)	1.338 (9)
C(13)–C(14)	1.373 (7)	C(68)–C(69)	1.407 (9)
C(14)–C(15)	1.391 (7)	C(69)–C(70)	1.378 (9)
C(14)–C(18)	1.508 (7)	C(70)–C(65)	1.355 (9)
C(15)–C(16)	1.390 (7)	Cl(3)–C(71)	1.722 (8)
C(16)–C(11)	1.408 (6)	C(71)–C(72)	1.447 (10)
C(16)–C(19)	1.509 (7)	C(72)–C(73)	1.366 (10)
C(21)–C(22)	1.396 (7)	C(73)–C(74)	1.407 (11)
C(22)–C(23)	1.404 (7)	C(74)–C(75)	1.450 (12)
C(22)–C(27)	1.518 (7)	C(75)–C(76)	1.407 (11)
C(23)–C(24)	1.386 (7)	C(76)–C(71)	1.395 (12)

[a] The estimated standard deviations of the least significant digits are given in parentheses.

(85) Brennan, T. D.; Scheidt, W. R. *Acta Crystallogr., Sect. C* **1988**, *C44*, 478–82.

Table IX. Bond Angles in $[Fe(TMP)(4\text{-}NMe_2Py)_2]ClO_4 \cdot 2C_6H_5Cl$[a]

type	value, deg	type	value, deg	type	value, deg	type	value, deg
N(1)FeN(2)	90.08 (16)	C(11)C(16)C(15)	118.2 (5)	N(2)C(a4)C(m2)	125.5 (4)	C(45)C(46)C(49)	119.7 (5)
N(1)FeN(3)	179.45 (16)	C(11)C(16)C(19)	121.1 (4)	N(3)C(a5)C(b5)	109.7 (4)	N(5)C(51)C(52)	124.6 (5)
N(1)FeN(4)	90.13 (16)	C(15)C(16)C(19)	120.6 (4)	C(b5)C(a5)C(m2)	125.5 (4)	C(51)C(52)C(53)	119.8 (5)
N(1)FeN(5)	89.28 (16)	C(m2)C(21)C(22)	121.1 (4)	N(3)C(a5)C(m2)	124.3 (4)	C(52)C(53)C(54)	116.2 (5)
N(1)FeN(6)	89.81 (16)	C(m2)C(21)C(26)	118.3 (4)	N(3)C(a6)C(b6)	109.8 (4)	C(52)C(53)N(7)	122.9 (5)
N(2)FeN(3)	89.90 (16)	C(22)C(21)C(26)	120.5 (4)	C(b6)C(a6)C(m3)	125.6 (5)	C(54)C(53)N(7)	120.8 (5)
N(2)FeN(4)	179.56 (16)	C(21)C(22)C(23)	118.2 (5)	N(3)C(a6)C(m3)	124.5 (4)	C(53)C(54)C(55)	119.6 (5)
N(2)FeN(5)	90.19 (16)	C(21)C(22)C(27)	122.3 (5)	N(4)C(a7)C(b7)	109.3 (4)	C(54)C(55)N(5)	124.2 (5)
N(2)FeN(6)	91.04 (16)	C(23)C(22)C(27)	119.4 (5)	C(b7)C(a7)C(m3)	125.9 (4)	C(53)N(7)C(56)	119.2 (4)
N(3)FeN(4)	89.89 (16)	C(22)C(23)C(24)	122.1 (5)	N(4)C(a7)C(m3)	124.5 (4)	C(53)N(7)C(57)	121.1 (4)
N(3)FeN(5)	91.27 (16)	C(23)C(24)C(25)	118.0 (5)	N(4)C(a8)C(b8)	109.2 (4)	C(56)N(7)C(57)	119.7 (4)
N(3)FeN(6)	89.64 (16)	C(23)C(24)C(28)	121.3 (5)	C(b8)C(a8)C(m4)	125.3 (5)	N(6)C(58)C(59)	124.2 (5)
N(4)FeN(5)	89.42 (16)	C(25)C(24)C(28)	120.6 (5)	N(4)C(a8)C(m4)	125.2 (5)	C(58)C(59)C(60)	120.1 (5)
N(4)FeN(6)	89.35 (16)	C(24)C(25)C(26)	122.4 (5)	C(a1)C(b1)C(b2)	107.3 (4)	C(59)C(60)C(61)	115.6 (5)
N(5)FeN(6)	178.47 (16)	C(21)C(26)C(25)	118.8 (5)	C(a2)C(b2)C(b1)	107.9 (4)	C(59)C(60)N(8)	123.3 (5)
FeN(1)C(a1)	126.2 (3)	C(21)C(26)C(29)	120.8 (4)	C(a3)C(b3)C(b4)	107.7 (5)	C(61)C(60)N(8)	121.1 (5)
FeN(1)C(a2)	127.1 (3)	C(25)C(26)C(29)	120.4 (5)	C(a4)C(b4)C(b3)	107.2 (4)	C(60)C(61)C(62)	119.8 (5)
C(a1)N(1)C(a2)	106.7 (4)	C(m3)C(31)C(32)	116.6 (4)	C(a5)C(b5)C(b6)	107.2 (4)	C(61)C(62)N(6)	125.2 (4)
FeN(2)C(a3)	126.8 (3)	C(m3)C(31)C(36)	123.4 (4)	C(a6)C(b6)C(b5)	107.4 (4)	C(60)N(8)C(63)	121.2 (5)
FeN(2)C(a4)	127.3 (3)	C(32)C(31)C(36)	120.0 (5)	C(a7)C(b7)C(b8)	107.5 (4)	C(60)N(8)C(64)	120.6 (5)
C(a3)N(2)C(a4)	105.8 (4)	C(31)C(32)C(33)	119.5 (5)	C(a8)C(b8)C(b7)	107.6 (4)	C(63)N(8)C(64)	118.1 (4)
FeN(3)C(a5)	127.3 (3)	C(31)C(32)C(37)	120.7 (4)	C(a2)C(m1)C(a3)	123.4 (5)	O(1)Cl(1)O(2)	110.3 (3)
FeN(3)C(a6)	126.8 (3)	C(33)C(32)C(37)	119.8 (5)	C(a2)C(m1)C(11)	120.4 (4)	O(1)Cl(1)O(3)	109.9 (3)
C(a5)N(3)C(a6)	105.8 (4)	C(32)C(33)C(34)	122.0 (5)	C(a3)C(m1)C(11)	116.1 (4)	O(1)Cl(1)O(4)	109.4 (3)
FeN(4)C(a7)	126.6 (3)	C(33)C(34)C(35)	117.9 (5)	C(a4)C(m2)C(a5)	122.9 (4)	O(2)Cl(1)O(3)	109.1 (3)
FeN(4)C(a8)	126.9 (3)	C(33)C(34)C(38)	119.8 (5)	C(a4)C(m2)C(21)	116.6 (4)	O(2)Cl(1)O(4)	109.5 (3)
C(a7)N(4)C(a8)	106.3 (4)	C(35)C(34)C(38)	122.1 (5)	C(a5)C(m2)C(21)	120.4 (4)	O(3)Cl(1)O(4)	108.6 (3)
FeN(5)C(51)	121.85 (24)	C(34)C(35)C(36)	121.7 (5)	C(a6)C(m3)C(a7)	123.5 (4)	Cl(2)C(65)C(66)	117.3 (6)
FeN(5)C(55)	122.57 (24)	C(31)C(36)C(35)	119.0 (5)	C(a6)C(m3)C(31)	115.8 (4)	C(65)C(66)C(67)	117.7 (6)
C(51)N(5)C(55)	115.5 (3)	C(31)C(36)C(39)	120.4 (4)	C(a7)C(m3)C(31)	120.7 (4)	C(66)C(67)C(68)	120.1 (7)
FeN(6)C(58)	123.26 (24)	C(35)C(36)C(39)	120.5 (5)	C(a8)C(m4)C(a1)	123.3 (4)	C(67)C(68)C(69)	120.2 (7)
FeN(6)C(62)	121.41 (24)	C(m4)C(41)C(42)	119.3 (4)	C(a8)C(m4)C(41)	119.7 (4)	C(68)C(69)C(70)	121.0 (7)
C(58)N(6)C(62)	114.9 (3)	C(m4)C(41)C(46)	121.5 (4)	C(a1)C(m4)C(41)	116.9 (4)	C(69)C(70)C(65)	117.0 (7)
N(1)C(a1)C(b1)	108.7 (4)	C(42)C(41)C(46)	119.2 (5)	C(m1)C(11)C(12)	119.4 (4)	C(70)C(65)C(66)	123.8 (6)
C(b1)C(a1)C(m4)	125.6 (5)	C(41)C(42)C(43)	119.3 (5)	C(m1)C(11)C(16)	120.0 (4)	C(70)C(65)Cl(2)	118.9 (6)
N(1)C(a1)C(m4)	125.2 (4)	C(41)C(42)C(47)	120.5 (5)	C(12)C(11)C(16)	120.2 (5)	Cl(3)C(71)C(72)	119.0 (6)
N(1)C(a2)C(b2)	109.3 (4)	C(43)C(42)C(47)	120.2 (5)	C(11)C(12)C(13)	119.2 (5)	C(71)C(72)C(73)	120.1 (7)
C(b2)C(a2)C(m1)	125.7 (5)	C(42)C(43)C(44)	122.0 (5)	C(11)C(12)C(17)	120.9 (5)	C(72)C(73)C(74)	120.4 (9)
N(1)C(a2)C(m1)	124.6 (4)	C(43)C(44)C(45)	117.5 (5)	Cl(13)C(12)C(17)	119.9 (5)	C(73)C(74)C(75)	118.8 (8)
N(2)C(a3)C(b3)	109.1 (4)	C(43)C(44)C(48)	120.6 (5)	C(12)C(13)C(14)	121.6 (5)	C(74)C(75)C(76)	121.7 (9)
C(b3)C(a3)C(m1)	125.1 (5)	C(45)C(44)C(48)	121.9 (5)	C(13)C(14)C(15)	118.4 (5)	C(75)C(76)C(71)	117.0 (8)
N(2)C(a3)C(m1)	125.5 (4)	C(44)C(45)C(46)	122.4 (5)	C(13)C(14)C(18)	121.5 (5)	C(76)C(71)C(72)	121.9 (7)
N(2)C(a4)C(b4)	110.3 (4)	C(41)C(46)C(45)	119.2 (5)	C(15)C(14)C(18)	120.1 (5)	C(76)C(71)Cl(3)	119.1 (6)
C(b4)C(a4)C(m2)	124.1 (5)	C(41)C(46)C(49)	121.1 (5)	C(14)C(15)C(16)	122.3 (5)		

[a] The estimated standard deviations of the least significant digits are given in parentheses.

$(OEP)(4\text{-}NMe_2Py)_2]ClO_4$ and the two ions of $[Fe(TMP)(1\text{-}MeIm)_2]ClO_4$ have relatively planar porphyrin cores. The S_4-ruffled core is a new feature of *meso*-mesitylporphyrin derivatives; the three previously reported TMP complexes, $[Cu(TMP^{\bullet})]$,[86] $[Zn(TMP)(H_2O)]$,[87] and $[Ru(TMP)(THF)(N_2)]$,[88] all have planar porphinato cores. The dihedral angles between the core and the four mesityl groups in $[Fe(TMP)(4\text{-}NMe_2Py)_2]ClO_4$ are 82.8, 69.9, 78.2, and 84.0°; all values are within the range suggested[89] as normal for tetraphenylporphyrin derivatives. The analogous angles in crystalline $[Fe(TMP)(1\text{-}MeIm)_2]ClO_4$ are 82.3, 89.7, 77.7, and 75.1°.

A well-defined symmetrical ligand binding pocket is formed by the 2- and 6-methyl substituents in the planar $[Fe(TMP)(1\text{-}MeIm)_2]ClO_4$ molecules (cf. Figure 3); the approximate depth of the pockets are 2.51 Å (molecule 1) and 2.45 Å (molecule 2). These dimensions are comparable to the values found previously.[87] However, the S_4-ruffling of the core in $[Fe(TMP)(4\text{-}NMe_2Py)_2]ClO_4$ leads to large variation in the position of the 2- and 6-methyl carbon atoms above the mean porphinato plane. There are effectively two classes of methyl groups: one group has an average perpendicular distance of 1.40 Å from the mean porphyrin plane, while the second has an average distance of 3.25 Å. The unequal distances of the methyl groups and the resulting shape of the ligand binding cavity are related to the orientation of the axial pyridine rings.

Discussion

Pyridines were chosen as the primary axial ligand for the steric reasons described below. In particular, 4-(dimethylamino)pyridine ($pK_a(BH^+) = 9.70$)[90] was chosen for this study because it is a strongly basic pyridine. Although there may also be significant effects by the porphyrin ligand on spin state,[91] the primary determinant of spin state in iron porphyrinates is the axial ligands.[92] Strongly basic ligands (including pyridines with $pK_a(BH^+) > 8.0$) normally yield complexes with the well-known rhombic low-spin iron(III) EPR spectrum.[38] Less basic pyridine ligands ($6.5 > pK_a(BH^+) > 5.0$) still yield low-spin ferric porphyrinates;[38,59] however, these species have a somewhat different electronic state and display a large g_{max} EPR feature with $g > 3.3$.[38,59] Some complexes with very weakly basic pyridine ligands ($pK_a(BH^+) < 3.0$) exhibit admixed intermediate-spin states with axial EPR spectra having $g_{\perp} > 4$.[93-95] On the basis of earlier studies of

(86) Song, H.; Reed, C. A.; Schedit, W. R. *J. Am. Chem. Soc.* **1989**, *111*, 6865-66.
(87) Song, H.; Scheidt, W. R. *Inorg. Chim. Acta* **1990**, *173*, 37-41.
(88) Camenzind, M. J.; James, B. R.; Dolphin, D.; Sparapany, J. W.; Ibers, J. A. *Inorg. Chem.* **1988**, *27*, 3054-57.
(89) Scheidt, W. R.; Lee, Y. J. *Struct. Bonding (Berlin)* **1987**, *64*, 1-70.
(90) Albert, A. In *Physical Methods in Heterocyclic Chemistry*; Katritzky, A. R., Ed.; Academic Press: New York, **1963**; Vol I, pp 1-108.
(91) Geiger, D. K.; Scheidt, W. R. *Inorg. Chem.* **1984**, *23*, 1970-72.
(92) Scheidt, W. R.; Reed, C. A. *Chem. Rev.* **1981**, *81*, 543-55.
(93) Scheidt, W. R.; Geiger, D. K.; Hayes, R. G.; Lang, G. *J. Am. Chem. Soc.* **1983**, *105*, 2625-32.

$[Fe(TPP)L_2]Cl$ in frozen solution,[38] the expected species formed with iron(III) porphyrinates and 4-(dimethylamino)pyridine is a low-spin complex displaying a normal rhombic EPR signal. This is the case for $[Fe(OEP)(4\text{-}NMe_2Py)_2]ClO_4$ in both frozen solution and in the crystalline form, but not for $[Fe(TMP)(4\text{-}NMe_2Py)_2]ClO_4$, which exhibits large g_{max} EPR spectra in both crystalline form and frozen solution. Clearly, porphyrin substituents play an important role in determining the type of EPR spectrum observed (and presumably also ligand orientation), as will be discussed below.

We first consider the molecular structure of the complexes. The overall conformation of $[Fe(TMP)(4\text{-}NMe_2Py)_2]ClO_4$ (Figures 3 and 6) is striking on two counts: the perpendicular relative orientation of the axial ligands and the strongly S_4-ruffled porphyrin core. We believe that both of these features are important components of axial ligand orientation control that is exerted in this "hindered" porphyrin system. Both features are manifestations of a set of subtle steric effects in the Fe^{III} (TMP) system. As we have noted previously,[93] low-spin pyridine complexes must have an orientation angle ϕ near 45° in order to avoid unfavorable steric interactions between the pyridine α-hydrogen atoms and porphyrin core atoms. This requirement is met in $[Fe(TMP)(4\text{-}NMe_2Py)_2]ClO_4$ where, as has already been noted, the absolute ϕ angles are 37 and 42°. Of course, orientation angles near 45° place the pyridine plane along $Fe\text{–}C_m$ vectors. This in turn leads to nonbonded repulsion between the methyl groups of the peripheral mesityl substituents and pyridine. Such nonbonded contacts in $[Fe(TMP)(4\text{-}NMe_2Py)_2]ClO_4$ are minimized by a tipping of the mesityl groups away from the pyridine ring. However, such tipping of the mesityl rings (approximately perpendicular to the mean porphinato plane) also requires substantial alteration in the position of the *meso*-carbon atoms of the porphyrin ring. The constraints of the cyclic porphyrin ligand will, in general, respond with an alternation in the displacements of the *meso*-carbon atoms and an overall D_{2d}-ruffled conformation. The nature of the required tippings of the mesityl groups is shown in Figure 9a. A movement of the mesityl ring methyl groups labeled 2 and 2′ away from the pyridine ring at the bottom of the figure is seen to alleviate the nonbonded interactions. However, it is also seen that such tipping would result in severe steric interaction with the pyridine ligand on the other side *if* the pyridines are coplanar. A rotation of the upper pyridine by 90° resolves this problem. Thus, the net result is ligand binding cavities on the two sides of the porphyrin ring that differ by ~90° in relative orientation.

These ideas of axial ligand orientation control are confirmed by the structures of $[Fe(OEP)(4\text{-}NMe_2Py)_2]ClO_4$ and $[Fe(TMP)(1\text{-}MeIm)_2]ClO_4$, which can be regarded as "control" molecules. The structure of $[Fe(OEP)(4\text{-}NMe_2Py)_2]ClO_4$ has the expected parallel relative orientation of the axial 4-(dimethylamino)pyridine ligands; indeed, precisely parallel ligands are required by the imposed crystallographic inversion symmetry. The ϕ orientation angle of the complex has the near 45° value expected for all pyridine derivatives; the observed value is 36°.

The nonbonded interaction between the methyl groups of the peripheral mesityls and the axial imidazole ligands in the two $[Fe(TMP)(1\text{-}MeIm)_2]ClO_4$ complexes are within acceptable limits even though the porphyrin remains effectively planar with no substantial movement of the mesityl groups. The two independent complexes, each with crystallographically required inversion symmetry, have ϕ angles of 23° for molecule 1 and 42° for molecule 2. These interactions are minimized in molecule 1 by the noncoplanarity of the imidazole and mesityl planes. Molecule 2, on the other hand, does have the imidazole ligands and two mesityl groups essentially coplanar. The arrangement is illustrated in Figure 9b. Unique methyl carbon to imidazole α-carbon atom distances are ~4 Å. The analogous distances in the *hypothetical* complex in which the imidazole ligands are replaced by pyridine

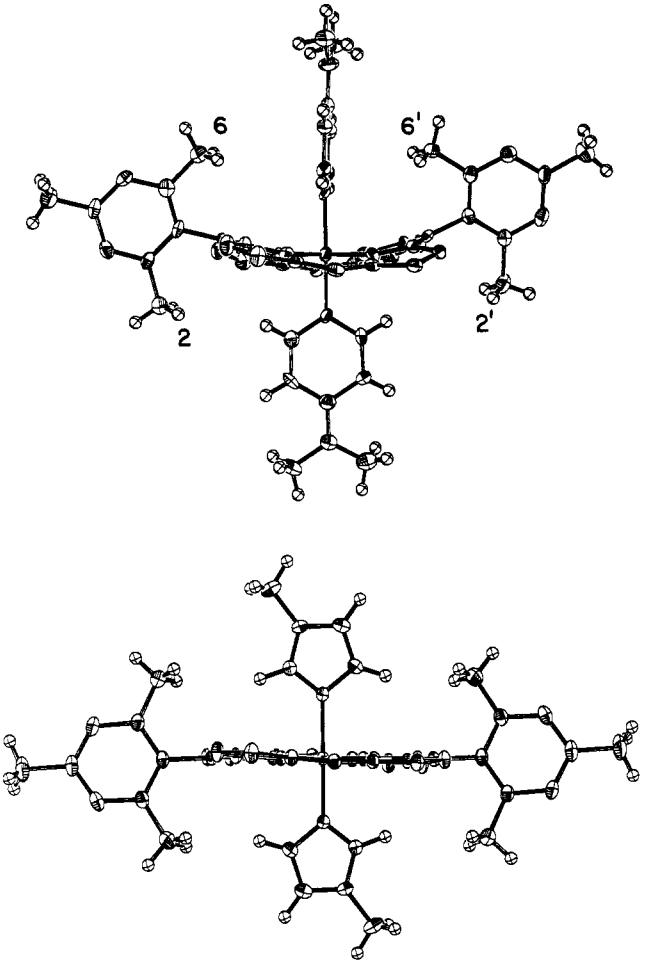

Figure 9. ORTEP diagrams showing the arrangement of the effectively coplanar mesityl rings and the axial ligands in (a) $[Fe(TMP)(4\text{-}NMe_2Py)_2]ClO_4$ and (b) molecule 2 of $[Fe(TMP)(1\text{-}MeIm)_2]ClO_4$. Hydrogen atoms have been drawn artificially small to improve clarity.

are about 0.3 Å shorter and hence somewhat repulsive. Figure 9a,b also shows the experimentally defined orientation of the hydrogen atoms; all 16 unique 2- and 6-mesityl methyl groups are the same. This methyl orientation provides a "geared" interaction with the axial ligand when the two are close together (cf. especially Figure 9b).

There is another distinct difference in the two $[Fe(TMP)(1\text{-}MeIm)_2]ClO_4$ structures that is related to the axial ligand orientation. The crystallographically unique $Fe\text{–}N_p$ bonds are experimentally different in molecule 1: 1.974 (2) and 2.002 (3) Å (see Figure 7). The $Fe\text{–}N_p$ bond that is close to being perpendicular to the projected imidazole plane is found to be shorter than the $Fe\text{–}N_p$ bond that is approximately parallel to the projected imidazole plane. Such rhombicity in the equatorial $Fe\text{–}N_p$ bonds was first noted for the structure of $[Fe(TPP)(HIm)_2]Cl\cdot CHCl_3\cdot H_2O$.[66] This rhombicity is believed to be the result of π-bonding effects. The axial ligand and porphyrin can both π-donate to the half-filled d_π orbital that is approximately perpendicular to the imidazole plane.[37] The other d_π orbital is filled, and hence no porphyrin → Fe π-donation can occur. As expected from this model, the two $Fe\text{–}N_p$ bond distances in molecule 2 are experimentally equal (1.987 (2) and 1.986 (2) Å) since the projection of the imidazole plane onto the porphinato core is almost equidistant to adjacent $Fe\text{–}N_p$ bonds and hence the two $Fe\text{–}N_p$ bonding interactions should be equivalent. Also as expected, the two distinct sets of bonds in molecule 1 have the same *average* value as that found in molecule 2.

The observed average $Fe\text{–}N_p$ bond distance of 1.964 Å in $[Fe(TMP)(4\text{-}NMe_2Py)_2]ClO_4$ is decidedly shorter than the 1.990-Å value given by Scheidt and Reed[92] as the expected value for bisligated low-spin iron(III) porphyrinates. The shortened

(94) Scheidt, W. R.; Safo, M. K. Unpublished results.
(95) Scheidt, W. R.; Osvath, S. R.; Lee, Y. J.; Reed, C. A.; Shaevitz, B.; Gupta, G. P. *Inorg. Chem.* **1989**, *28*, 1591–95.

Table X. Summary of Fe–N Bond Distances, Core Conformation, and Ligand Orientation in Low-Spin Six-Coordinate Pyridine and Imidazole Derivatives

complex	$Fe-N_p$[a]	$Fe-N_{ax}$[a,b]	C_m[c,d]	C_b[c,d]	C_{av}[c,d]	C_{max}[d,e]	ϕ[f]	$\Delta\phi$[f]	ref
[K(K222)][Fe(BH(Bipy)$_2$P)(CN)$_2$](H$_2$O)$_3$·$^1/_2$C$_6$H$_5$F	1.949 (14)	NA	64 (7)	24 (16)	30	73	NA	NA	98
[Fe(TMP)(4-NMe$_2$Py)$_2$]ClO$_4$	1.964 (10)	1.989 (4)	51 (5)	20 (13)	25	57	37	79	this work
		1.978 (4)					42		
[Fe(TPP)(2-MeHIm)$_2$]ClO$_4$	1.971 (4)	2.015 (4)	40 (1)	17 (16)	21	41	32	89	105
		2.010 (4)					32		
[Fe(TPP)(CN)(Py)]	1.970 (14)	2.075 (3)	38 (7)	23 (16)	22	41	40		108a
[Fe(TPP)(NCS)(Py)]	1.988 (9)	2.082 (2)	35 (6)	22 (15)	20	40	39		99
[Fe(TPP)(N$_3$)(Py)]	1.989 (6)	2.089 (6)	29 (5)	21 (12)	17	35	40		100
[Fe(TPP)(HIm)$_2$]Cl·MeOH	1.989 (8)	1.991 (5)	31 (3)	12 (9)	16	33	18	57	106
		1.957 (4)					39		
[Fe(OEP)(CN)(Py)]	1.980 (4)	2.087 (3)	29 (6)	13 (7)	15	35	31		108b
[Fe(TPP)(Py)$_2$]ClO$_4$	1.982 (7)	2.005 (5)	25 (4)	14 (11)	14	29	34	86	59
		2.001 (5)					38		
[Fe(T2,6-Cl$_2$PP)(1-VinIm)$_2$]ClO$_4$	1.978 (8)	1.976 (4)	22 (3)	9 (9)	11	26	5	6, 76	56
		1.968 (4)					14		
							20		
[Fe(TPP)(1-MeIm)$_2$]ClO$_4$	1.982 (11)	1.970 (3)	9 (5)	23 (5)	12	31	22	11	67
		1.978 (3)					32		
[Fe(TpivPP)(NO$_2$)(HIm)]	1.970 (4)	2.037 (5)	20 (4)	9 (6)	9	22	16	69	103
							53		
[Fe(TpivPP)(NO$_2$)(Py)]	1.983 (3)	2.093 (5)	14 (4)	11 (7)	10	20	24	77	103
							53		
[Fe(Proto IX)(1-MeIm)$_2$]	1.991 (16)	1.988 (5)	14 (2)	7 (4)	7	13	3	13	107
		1.966 (5)					16		
[Fe(TMP)(1-MeIm)$_2$]ClO$_4$	1.988 (20)	1.975 (3)	1 (1)	2 (2)	1	4	23	0	this work
	1.987 (1)	1.965 (3)	8 (1)	7 (2)	5	9	41	0	this work
[Fe(OEP)(4-NMe$_2$Py)$_2$]ClO$_4$	2.002 (4)	1.995 (3)	6 (5)	6 (4)	5	10	36	0	this work
K[Fe(TPP)(CN)$_2$]	2.000 (6)	NA	4 (10)	4 (2)	3	6	NA	NA	101
[Fe(OEP)(3-ClPy)$_2$]ClO$_4$	1.995 (6)	2.031 (2)	3 (1)	4 (2)	3	6	41	0	112
[Fe(TPP)(HIm)$_2$]Cl·CHCl$_3$	1.994 (12)	1.977 (3)	0 (0)	2 (1)	1	4	6	0	66
	1.993 (4)	1.964 (3)	4 (4)	2 (2)	2	7	41	0	66
[Fe(TPP)(*c*-MU)$_2$]SbF$_6$	1.995 (17)	1.979 (7)	4 (1)	2 (3)	3	6	16	0	68
	1.997 (1)	1.967 (7)	2 (1)	1 (1)	1	2	29	0	68
[Fe(TPP)(*t*-MU)$_2$]SbF$_6$	1.992 (5)	1.983 (4)	1 (0)	2 (1)	2	4	22	0	68
[K(18C6)][Fe(TpivPP)(NO$_2$)$_2$]	1.992 (1)	NA	3 (0)	1 (1)	2	3	NA	NA	102

[a] Values in angstroms. [b] N_{ax} is either a substituted pyridine or imidazole ligand. [c] Average absolute value of displacements of the methine carbons (C_m), β-carbons (C_b), and the 24-atom (C_{av}) from the 24-atom core plane. [d] Values in units of 0.01 Å. [e] Maximum absolute displacement of any core atom from the 24-atom core plane. [f] Values in degrees.

equatorial distances are the result of the core ruffling; as originally noted by Hoard,[96,97] an S_4-ruffling of the core leads to shorter $M-N_p$ bond distances compared to the analogous species with planar porphyrin cores. Since the time of the Scheidt and Reed review,[92] there have been a number of bis-ligated low-spin iron(III) structures determined.[56,98-103] Parameters from these have been tabulated in Table X. In order to demonstrate the effects of core ruffling on the $Fe-N_p$ bond distances, these complexes have been approximately ordered in terms of decreased *ruffling* of the porphinato core. The correlation of $Fe-N_p$ distance and core conformation are evident. Measures of core ruffling are provided by the listed deviations, from the mean porphinato core, of the C_m, C_b, C_{av}, and C_{max} groups of atoms. It is interesting to note that all of the neutral nitrogen donor complexes that exhibit the large g_{max} EPR signal are found to have significantly ruffled porphinato cores. The significance of this observation is unclear at this time. Of the two dicyanoiron(III) complexes thus far reported, the core of K[Fe(TPP)(CN)$_2$] is not ruffled,[108] yet gives a large g_{max} EPR signal,[59] while that for [K(222)][Fe(BH(Bipy)$_2$P)(CN)$_2$] is severely ruffled, "...probably mainly due to the presence of the cyanide axial ligands and their steric interactions with the bipyridine handles..."[98] of the this basket handle porphyrin complex. Both [Fe(TMP)(1-MeIm)$_2$]ClO$_4$ and [Fe(OEP)(4-NMe$_2$Py)$_2$]ClO$_4$ have effectively planar cores, and as shown in Table X, their equatorial $Fe-N_p$ bond distances are seen to be in accord with this class of iron(III) species.

The axial bond distances are also tabulated in Table X. The axial Fe–N(Im) bond distances in [Fe(TMP)(1-MeIm)$_2$]ClO$_4$ show the correlation with imidazole orientation that has been noted previously; namely, the smaller axial distance is associated with the larger value of ϕ. However, the value of ϕ is not a useful predictor of the absolute value of Fe–N(Im) distance for the various imidazole complexes reported in Table X. The axial Fe–N(4-NMe$_2$Py) bond distances in the two complexes reported here have somewhat different values; we are uncertain why this is so. The distances in both complexes are shorter than those seen in either the bis(pyridine) or mixed-ligand complexes of known structure.

From the g values measured by EPR spectroscopy and confirmed by Mössbauer spectroscopy (Figure 2b) for [Fe(OEP)(4-NMe$_2$Py)$_2$]ClO$_4$, the crystal field parameters V/λ and Δ/λ have been calculated. For [Fe(TMP)(4-NMe$_2$Py)$_2$]ClO$_4$ the same

(96) Hoard, J. L. *Ann. N.Y. Acad. Sci.* **1973**, *206*, 18–31.
(97) Collins, D. M.; Scheidt, W. R.; Hoard, J. L. *J. Am. Chem. Soc.* **1972**, *94*, 6689–96.
(98) Schappacher, M.; Fisher, J.; Weiss, R. *Inorg. Chem.* **1989**, *28*, 389–90.
(99) Scheidt, W. R.; Lee, Y. J.; Geiger, D. K.; Taylor, K.; Hatano, K. *J. Am. Chem. Soc.* **1982**, *104*, 3367–74.
(100) Adams, K. M.; Rasmussen, P. G.; Scheidt, W. R.; Hatano, K. *Inorg. Chem.* **1979**, *18*, 1892–99.
(101) Scheidt, W. R.; Haller, K. J.; Hatano, K. *J. Am. Chem. Soc.* **1980**, *102*, 3017–21.
(102) Nasri, H.; Goodwin, J. A.; Scheidt, W. R. *Inorg. Chem.* **1990**, *29*, 185–91.
(103) Nasri, H.; Wang, Y.; Huynh, B. H.; Walker, F. A.; Scheidt, W. R. *Inorg. Chem.*, in press.
(104) Migita, C. T.; Iawizumi, M. *J. Am. Chem. Soc.* **1981**, *103*, 4378–81.
(105) Scheidt, W. R.; Kirner, J. L.; Hoard, J. L.; Reed, C. A. *J. Am. Chem. Soc.* **1987**, *109*, 1963–68.
(106) Collins, D. M.; Countryman, R.; Hoard, J. L. *J. Am. Chem. Soc.* **1972**, *94*, 2066–72.
(107) Little, R. G.; Dymock, K. R.; Ibers, J. A. *J. Am. Chem. Soc.* **1975**, *97*, 4532–39.
(108) (a) Scheidt, W. R.; Lee, Y. J.; Luangdilok, W.; Haller, K. J.; Anzai, K.; Hatano, K. *Inorg. Chem.* **1983**, *22*, 1516–22. (b) Scheidt, W. R.; Hatano, K. *Acta Crystallogr., Sect. C*, in press.

parameters have been estimated by a combination of EPR and Mössbauer spectroscopies (Figure 2a and comments in the Results). The two sets of values estimated from the Mössbauer spectra fits of the latter compound are listed in Table VII. In either case, V/λ is small (0.7 or 0.89). The major difference in the parameters derived from the two fits are the values of Δ/λ and A_y. We have no independent way of estimating A_y. As for Δ/λ, which is considered to be a measure of ligand field strength or basicity, there are reasons for preferring either the smaller (1.9) or the larger (3.6) value. On the one hand, the smaller value of Δ/λ represents the unconstrained Mössbauer fit parameters and may indicate some role for the ruffling of the porphyrin ring and/or basicity differences between TMP and other commonly used porphyrin ligands in decreasing the values of Δ/λ. On the other hand, the larger (constrained) value of Δ/λ represents consistency with the values of Δ/λ obtained for other bis[4-(dimethylamino)pyridine]iron(III) complexes (admittedly all of which have apparently mutually parallel ligand planes, based on their EPR spectra) and with the expected stronger ligand field of 4-NMe_2Py relative to pyridine itself,[59] porphyrin basicity effects aside. The present Mössbauer spectra do not allow us to distinguish between these two possibilities. Because of the potential importance of ruffling of the porphyrin ring and/or basicity differences between TMP and other commonly used porphyrins on the crystal field and hyperfine parameters, single-crystal EPR investigations of a series of $[Fe(TMP)(L)_2]^+$ complexes are planned. In any case, from the present results it is clear that the near-degeneracy of d_{xz} and d_{yz} (small value of V) for $[Fe(TMP)(4\text{-}NMe_2Py)_2]ClO_4$ is clearly diagnostic of a perpendicular orientation of planar axial ligands and inconsistent with a parallel orientation of the axial ligands that leads to much larger values of V/λ, as seen for the case of $[Fe(OEP)(4\text{-}NMe_2Py)_2]ClO_4$ (Table VII).

An important finding of the present study is that the effects of parallel vs perpendicular axial ligand orientation are also manifested in the quadrupole splittings in zero field at 77 K. An examination of the data summarized in Table VI shows that all complexes with known perpendicular axial ligand orientations have ΔE_q less than 1.8 mm/s while those with known parallel orientations have ΔE_q greater than 2.1 mm/s. Thus, a relatively simple Mössbauer experiment has the potential of providing an easy diagnostic test for relative ligand plane orientations. Medhi and Silver[72] have recently discussed the crystal field rationale for such dependence of the quadrupole splitting constant on geometry. In addition, they have reported Mössbauer measurements at 80 K of a variety of complexes in frozen DMSO solution.

The crystallographic, EPR, and Mössbauer results presented herein confirm, for bis(pyridine) complexes, our earlier conclusion, based on studies of bis(imidazole) complexes,[41,56] that there is a direct correspondence between the type of EPR spectrum observed (normal rhombic vs large g_{max}) and the relative orientation of planar axial ligands (parallel vs perpendicular). In the absence of steric effects of the porphyrin macrocycle, as in the OEP complex, the strongly basic pyridine 4-NMe_2Py prefers to bind with the two ligands in parallel planes. The EPR spectrum, observed at 77 K and below in both polycrystalline form and in frozen solution, is a normal rhombic spectrum as was observed previously for the TPP complexes in frozen solution.[38] When the porphyrin contains substituents that sterically hinder the strongly basic pyridine ligands from being in parallel planes, as in the TMP complex, they align themselves in perpendicular planes and the EPR spectrum switches to a large g_{max} type. As in the case of $[Fe(TPP)(2\text{-}MeHIm)_2]Cl$,[41] Mössbauer spectroscopy again provides a means of estimating the unobserved g-values.

Basic pyridines such as 4-(dimethylamino)pyridine ($pK_a(BH^+)$ = 9.70) have been shown to be fairly strong π-donors as well as strong σ-donors.[109] Such ligands (basic pyridines and nonhindered imidazoles) have been shown to prefer parallel alignment so that both ligands can be involved in L → M π-back-donation to the hole that is, in this case, localized mainly in one of the dπ (either d_{xz} or d_{yz}) orbitals of low-spin iron(III). This is thus a case in which parallel alignment is stabilized by ligand field effects, as earlier suggested by Strouse.[59] On the other hand, weakly basic pyridines such as pyridine itself ($pK_a(BH^+)$ = 5.20) are considered to be weak π-donors as well as weak σ-donors,[109,110] thereby decreasing the tendency for L → M π-donation and parallel ligand orientation. Hence, weakly basic pyridines typically produce complexes that give rise to large g_{max} EPR spectra and have been shown, in the case of $[Fe(TPP)(Py)_2]ClO_4$,[59] to have the axial ligands in perpendicular planes. Single-crystal EPR spectroscopy of the latter complex allowed measurement of all three g values and their orientations: $g_x = -0.46$, $g_y = 1.12$, and $g_z = 3.70$, where g_z is along the axial direction of the complex.[59] These values are similar to those found by a combination of EPR and Mössbauer spectroscopies in this study for $[Fe(TMP)(4\text{-}NMe_2Py)_2]ClO_4$, where the basic pyridine is forced to take on a perpendicular alignment of axial ligands because of the steric effects of the TMP ligand.

A case that appears to have closely balanced the steric requirements of the porphyrin ligand and the π-bonding preference of the pyridine is that of the $[Fe(T2,6\text{-}Cl_2PP)(4\text{-}NMe_2Py)_2]ClO_4$ complex. In frozen methylene chloride solution at 24 K, this complex shows only a large g_{max} EPR spectrum, with $g = 3.54$.[111] However, microcrystalline preparations of the complex show a rhombic EPR spectrum (Table V). Similar observations were made for $[Fe(T2,6\text{-}Cl_2PP)(4\text{-}NH_2Py)_2]ClO_4$.[111] It would thus appear that the T2,6-Cl_2PP ligand may provide slightly less steric bulk at the ortho positions of the phenyl rings than does the TMP ligand, such that although the lowest energy form (presumably that in frozen solution) is that in which the axial ligands are in perpendicular planes, crystal-packing forces are able to stabilize parallel forms of the complex. Such crystal-packing effects on ligand orientation have been documented for solid-state forms of $[Fe(OEP)(3\text{-}ClPy)_2]ClO_4$.[93,112] It would be interesting to solve the structure of a T2,6-Cl_2PP complex in order to see how the 2,6-dichlorophenyl groups are able to accommodate themselves with (parallel) pyridine ligands.

Acknowledgment. We thank the National Institutes of Health for support of this research under Grants GM-38401 (W.R.S.), HL-16860 to George Lang, and DK-31038 (F.A.W.). We also thank Prof. B. H. Huynh for many helpful discussions and for communicating results in advance of their publication.

Supplementary Material Available: Table SI, complete crystal data and intensity collection parameters, Tables SII and SIII, anisotropic thermal parameters and fixed hydrogen atom positions for $[Fe(OEP)(4\text{-}NMe_2Py)_2]ClO_4$, Tables SIV–SVI, anisotropic thermal parameters, fixed chlorobenzene atom positions, and fixed hydrogen atom positions for $[Fe(TMP)(4\text{-}NMe_2Py)_2]ClO_4$, Tables SVII and SVIII, anisotropic thermal parameters and fixed hydrogen atom positions for $[Fe(TMP)(1\text{-}MeIm)_2]ClO_4$, Tables SIX and SX, bond distances and angles for $[Fe(OEP)(4\text{-}NMe_2Py)_2]ClO_4$, Tables SXI and SXII, bond distances and angles for $[Fe(TMP)(1\text{-}MeIm)_2]ClO_4$ (24 pages); listings of observed and calculated structure factors (70 pages). Ordering information is given on any current masthead page.

(109) Ramsey, B. G.; Walker, F. A. *J. Am. Chem. Soc.* **1974**, *96*, 3314–16.
(110) Johnson, C. R.; Shepherd, R. E. *Inorg. Chem.* **1983**, *22*, 3506–13.
(111) Safo, M. K.; Scheidt, W. R.; Walker, F. A. Unpublished results.
(112) Scheidt, W. R.; Geiger, D. K.; Haller, K. J. *J. Am. Chem. Soc.* **1982**, *104*, 495–99.